Food Science WILEY

Hybrid mixture theory-based modeling of transport of fluids, species, and heat in food biopolymers subjected to freeze–thaw cycles

Ying Zhao[1] | Pavitra Krishna Kumar[2] | Shyam S. Sablani[2] | Pawan S. Takhar[3,*]

[1]Agricultural and Biological Engineering, University of Illinois at Urbana-Champaign, Urbana, Illinois, USA

[2]Biological Systems Engineering, Washington State University, Pullman, Washington, USA

[3]Food Science and Human Nutrition, University of Illinois at Urbana-Champaign, Urbana, Illinois, USA

Correspondence
Pawan S. Takhar, Food Science and Human Nutrition, University of Illinois at Urbana-Champaign, Urbana, IL 61801, USA.
Email: ptakhar@illinois.edu

*The author has previously published as Pawan P. Singh.

Abstract: A hybrid mixture theory (HMT)-based unsaturated transport (pores not saturated with liquid) model was applied to a food matrix subjected to freezing and freeze–thaw cycles. The model can explain the fluid, species, and heat transport, ice formation, thermomechanical changes, and the freezing point depression occurring inside food biopolymers during freezing. Volume changes during freezing were calculated using the stresses due to pore pressure and the phase-change based mechanical strain. The Eulerian-Lagrangian transformation was performed for solving the equations using a finite element mesh in Lagrangian coordinates. The predicted temperature profiles for constant and fluctuating freezing temperature conditions showed agreement with experimental data with reasonable accuracy (RMSE = 2.86°C and 2.23°C, respectively). The multiscale transport model coupled with a physical chemistry-based relation was able to predict solute concentration and the freezing point depression in potatoes with greater accuracy than an empirical equation published in the literature. Sudden temperature fluctuations representing the opening and closing of a freezer door were investigated using this solution scheme, and conditions causing less damage to the food were identified.

KEYWORDS
diffusion, freeze–thaw cycles, mathematical modeling, multiscale modeling

Practical Application: Food materials are subjected to freeze–thaw cycles during storage, shipping, and distribution to the consumers. The study uses numerical modeling and experimental validation to elucidate the principles affecting ice formation, solute migration, and temperature changes. Outcomes will allow processors to improve the quality of frozen foods with improved design of freezing operation, and storage and distribution strategies.

1 | INTRODUCTION

Freezing is commonly used for preserving product quality and extending the shelf life of food products. The global frozen foods market, expected to reach $300 billion by 2020, denotes the increasing consumer demand (Sharma, 2014). Maintenance of the foods' taste and quality are the main factors for the boost in the frozen food market since the freezing process can inhibit microbial growth, lower water activity, and decrease chemical and enzymatic reactions (Sun, 2016). Frozen foods can be shipped and stored without geographical limitations. However, the condition of the freezing process, as well as shipping and storage, plays a vital role in affecting the quality of frozen foods. A critical aspect of transport and storage for frozen products is freeze–thaw cycles. These cycles caused by the temperature variations during shipping and storage contribute to the fluid diffusion and ice recrystallization inside frozen foods (Adapa et al., 2000). These phenomena are the main contributors of quality deterioration, such as mass loss, and textural changes, which directly lead to economic losses in the frozen food industry.

Therefore, an in-depth understanding of the freezing mechanisms, ice formation/melting, solute and moisture migration, and heat transfer during freeze–thaw cycles is of great value. However, due to the complex and dynamic nature of the freezing process, purely experimental methods cannot be utilized to evaluate multiple factors affecting the transport mechanisms. By using mathematical modeling, complementary information can be obtained, and underlying mechanisms can be elucidated.

In the past freezing studies with foods, analytical approximations like Plank's equation have been used to predict freezing time (Heldman & Taylor, 1997; Pham, 1986). These approaches provide a good first approximation but are not able to account for complex freezing mechanisms (Delgado & Sun, 2001). Some researchers used numerical methods for modeling heat transfer and mass migration during freezing (Delgado & Sun, 2001). However, these heat transfer-based studies used only macroscale equations, which cannot adequately address the phenomena taking place at lower scales (Pham, 2006; Sun, 2016).

The multiscale characteristics can be explained using a frozen potato tissue (Figure 1). At microscale (of the order of microns), individual starch granules, protein polymers, and cell walls are present. At this scale, solid polymers and vicinal water are distinct, and ice nuclei start to form at crystallization sites during freezing. At mesoscale ($<10^3$ μm), the whole starch granules, ice crystals, and cell cytoplasm are present. The particle represents a mixture of biopolymers and vicinal fluid. The water migration and solute diffusion due to ice crystal formation also occur at
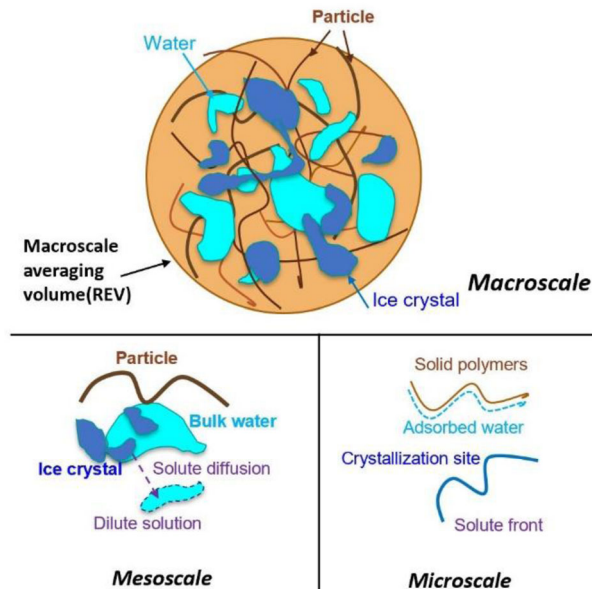

FIGURE 1 Multiscale nature of transport processes during freezing of a food material

this scale. Macroscale represents the mixture at a higher scale (of the order of centimeters). The macroscale representative elementary volume (REV) denotes the elementary volume representing the structure and composition at the macroscale point. The microscale changes can influence the material at the macroscale. For instance, ice expansion in amorphous lamellae or wall channels at the micro/mesoscale is caused by crystallization and recrystallization during freeze–thaw cycles. At the macroscale, the potato tubers have been observed to develop oblong scratches and solid wall ruptures by using atomic force microscopy and CT-scanning techniques (Szymońska & Wodnicka, 2005; Zhao & Takhar, 2017b).

The ice recrystallization in a product depends on the level of temperature fluctuations causing state and phase transitions in the product. Potatoes, along with other starch rich products are among robust products maintaining their quality during freeze–thaw cycles. The possible reason is—the characteristics of thermal transition temperatures, $T_{g'}$ and $T_{m'}$ of potatoes are around −11°C, and few degrees of temperature fluctuation, for example, the temperature fluctuation between −21°C and −13°C will induce minimal ice recrystallization resulting in marginal changes in structural damage as documented in our previous publication (Kumar et al., 2019). Potatoes were selected for this study to test the complex freezing process model in a product with more homogenous properties instead of the ones with heterogeneous properties.

Hybrid mixture theory (HMT) can be used to describe multiscale transport and thermomechanical mechanisms during the freezing process. HMT was developed using

the framework of continuum mechanics for porous materials to include the effect of physical mechanisms at lower scales on macroscale processes (Hassanizadeh & Gray, 1979). The field equations (laws of conservation of mass, momentum, energy and entropy) are formulated at the microscale and upscaled to meso- and macroscales using mathematical filtering theorems (Bennethum & Cushman, 1996), where the constitutive theory is formulated and the entropy inequality is exploited. The resulting laws are able to describe a physical process in a thermodynamically viable manner (Battiato et al., 2019). The earlier work was further developed for swelling/shrinking soils and food gels with short memory effects (Achanta et al., 1994). Takhar and coworkers initially developed HMT-based equations for biopolymeric materials with long memory effects subjected to saturated transport (Singh et al., 2003a, 2003b), and later for unsaturated transport mechanisms (Takhar, 2014). The unsaturated transport resulted in generalized Darcy's law, pressure relations, and thermomechanical equations for biopolymeric matrices. Using HMT, food processes with phase changes such as frying and expansion of polymers exiting an extruder have been successfully studied (Bansal et al., 2014, 2015; Ditudompo & Takhar, 2015). In phase change problems, the mass, momentum, and energy exchange between different phases is accounted for via source/sink terms of multiscale balance laws.

The objective of this study is to utilize the two-scale HMT-based equations to model transport of fluids (water and gas), heat, solute, and volume deformation during freezing. The two-scale approach merges the micro and mesoscale physics, assuming there is a continuum for adsorbed and bulk fluid phases. The air phase is expected to exist in frozen foods either by introduction during foaming or other reasons such as respiration in fruits and vegetables. Due to water-vapor pressure differences between the unfrozen water or ice and the air phase, they are expected to exchange water vapors. Thus, it becomes essential to include gas phase, which makes the system of unsaturated type. Vapor movement is considered as the main mechanism for moisture movement in frozen foods (Pham, 2016).

Here, we apply this unsaturated transport theory and also include the ice phase and solute transport equations. Thus, in the current study, there are two solid phases (ice and solid biopolymers). The ice phase exchanges mass with water and exhibits phase transition-based volume changes. The solid biopolymers exhibit viscoelastic behavior and do not exchange mass with other phases. Various phases exchange momentum, energy, and entropy with each other (Takhar, 2014). In addition, we also incorporate the species transport aspect of HMT to include diffusion of solutes in the food matrix subjected to freeze–thaw

cycles. This would allow calculating freezing point depression and solute concentration. In the previous HMT-based studies, the species transport was theoretically derived but not solved to describe a process (Bennethum & Cushman, 1996; Singh et al., 2003b). Volume expansion or shrinkage due to fluid motion and phase transitions is taken into account using poroelastic and thermomechanical equations. The equations are transformed from Eulerian to Lagrangian coordinates, and a stationary mesh is used for obtaining the solution using the finite element method. The solution obtained in Lagrangian coordinates is transformed back to the moving Eulerian coordinates. The validation and applications of the model are also demonstrated.

2 | MODEL FORMULATION

2.1 | Assumptions

The frozen material was considered as heterogeneous at length scales larger than the REV, in which the water, ice, and solid biopolymer phases were assumed to be incompressible at microscale. The gas-phase was assumed as an ideal mixture of vapors and dry air and was treated as compressible. When the ice was formed, its velocity relative to the solid biopolymers was assumed to be zero, which implies that ice could not migrate in a porous matrix. Ice content at different spatial locations could still change through the combined effect of phase change and migration of water and vapors to and from ice sites. The sublimation/condensation effect was ignored because the freezing conditions ($-20°C$ and ambient pressure) were away from the triple point of the water. All phases were at local thermal equilibrium inside the macroscale REV. The effect of gravity was neglected. The nucleation effect was included using initial conditions in the species transport equation as described below.

2.2 | Two-scale mass balance relations

In a multiphase system comprised of water, ice, and gas (air + vapor mixture), the two-scale mass balance for a phase α can be written as (Takhar, 2014):

$$\frac{D^s(\varepsilon^\alpha \rho^\alpha)}{Dt} + \nabla \cdot (\varepsilon^\alpha \rho^\alpha v^{\alpha,s}) - \frac{\varepsilon^\alpha \rho^\alpha}{\varepsilon^s}\frac{D^s \varepsilon^s}{Dt}$$
$$= \sum_{\substack{\beta=w,\,i,\,g \\ \beta \neq \alpha}} {}^\beta \hat{e}^\alpha \, where \, \alpha = w,\,i,\,g \quad (1)$$

To derive above equation, the following solid phase mass balance equation was utilized in a moving solid matrix $D^s \varepsilon^s / Dt + \varepsilon^s \nabla \cdot v^s = 0$. The solid biopolymers are

considered as incompressible at the microscale ($D^s \rho^s / Dt = 0$) with no mass exchange with other phases ($^\beta \hat{e}^\alpha = 0$ for solid biopolymers). Since the water can be assumed to be incompressible at the microscale, $D^s \rho^w / Dt = 0$ in Equation (1).

The ice phase is also incompressible; therefore, the ice phase equation can be obtained in a similar manner. Since ice can exchange water with the gas and water phases, the $^\beta \hat{e}^i$ for ice is not zero:

$$\rho^i \frac{D^s \varepsilon^i}{Dt} + \nabla \cdot \left(\rho^i \varepsilon^i v^{i,s} \right) - \frac{\varepsilon^i \rho^i}{\varepsilon^s} \frac{D^s \varepsilon^s}{Dt} = {}^g \hat{e}^i + {}^w \hat{e}^i \quad (2)$$

Since the gas phase is compressible at the microscale, it implies that $D^s \rho^g / Dt \neq 0$. The mass balance for the gas phase can be written as (Takhar, 2014):

$$\rho^g \frac{D^s \varepsilon^g}{Dt} + \varepsilon^g \frac{D^s \rho^g}{Dt} + \nabla \cdot (\rho^g \varepsilon^g v^{g,s}) - \frac{\varepsilon^g \rho^g}{\varepsilon^s} \frac{D^s \varepsilon^s}{Dt} = {}^w \hat{e}^g + {}^i \hat{e}^g \quad (3)$$

Using the ideal gas law, partial pressure of water vapors (P^v) was calculated from the vapor density ($P^v = \rho^v R^v T$). Moreover, components of the gas mixture share the same volume, so $\varepsilon^v = \varepsilon^g$. The vapor mass balance was used to obtain the density of vapors.

$$\rho^v \frac{D^s \varepsilon^v}{Dt} + \varepsilon^v \frac{D^s \rho^v}{Dt} + \nabla \cdot (\rho^v \varepsilon^v v^{v,s}) - \frac{\varepsilon^v \rho^v}{\varepsilon^s} \frac{D^s \varepsilon^s}{Dt} = {}^w \hat{e}^g + {}^i \hat{e}^g \quad (4)$$

The following restrictions apply to the volume fraction values for different phases. The sum of the macroscale volume fractions of different phases at each spatial location is equal to one. Thus,

$$\varepsilon^s + \varepsilon^w + \varepsilon^g + \varepsilon^i = 1 \quad (5)$$

The above equation also leads to $\dot{\varepsilon}^s + \dot{\varepsilon}^w + \dot{\varepsilon}^g + \dot{\varepsilon}^i = 0$, where dot represents D^s / Dt. The porosity can be calculated as the sum of volume fractions of water, ice, and gas phases ($\phi = \varepsilon^w + \varepsilon^g + \varepsilon^i$), which is also related to the solid phase volume fraction (ε^s) via $\varepsilon^s = 1 - \phi$.

2.3 | Momentum balance

In Equation (1), $v^{w,s}$ is the velocity of water relative to the solid phase. To calculate $v^{w,s}$, Takhar's (2014) generalized Darcy's law for isotropic biopolymers was used:

$$v^{w,s} = -\varepsilon^w \frac{K^w}{\mu^w} \nabla P^w - \varepsilon^w D^w \nabla \varepsilon^w - \varepsilon^w \frac{D^w}{E^w} N^w \nabla \dot{\varepsilon}^w \quad (6)$$

This equation combines Darcy's and Fick's laws in a single equation, which makes it suitable for fluid transport in biopolymers, as both pressure- and concentration-driven

flow can occur in them. The third term on RHS is the mixture viscosity force term, which incorporates viscous resistance of polymers affecting fluid flow.

In Equation (2), the ice velocity relative to a solid biopolymer was taken as zero ($v^{i,s} = 0$), which means ice could not migrate in a solid form and can only diffuse when it changes to water.

In Equation (3), the velocity of gas relative to solid can be written as:

$$v^{g,s} = -\varepsilon^g \frac{K^g}{\mu^g} \nabla P^g \quad (7)$$

In Equation (4), the vapor phase velocity is the summation of gas-phase velocity and vapor diffusive velocity: $v^{v,s} = v^{g,s} + v^{v,g}$. The diffusive vapor velocity is given by $v^{v,s} = -(D^{v/\omega v}) \nabla \omega^v$, which is the binary-diffusion equation for the mixture of vapors and air (Bird et al., 2007). Here, ω^v is the mass fraction of water vapors in the air–vapor mixture, which is given by $\omega^v = \rho^v / (\rho^v + \rho^a)$. Since gas is a mixture of vapor and air, Dalton's Law of partial pressures, $P^g = P^v + P^a$ can be utilized in the pores to calculate air pressure from total gas pressure and vapor partial pressure.

2.4 | Energy balance

During freezing of foods with initial temperature greater than the freezing temperature, both sensible and latent heat are removed. When the food's temperature reaches its freezing point, the fluid inside the matrix undergoes a phase change to form ice crystals, which subsequently increase in size. A two-scale convection–diffusion equation was used to calculate the heat transfer in the porous biomaterial (Bear & Bachmat, 2012; Bird et al., 2007; Takhar, 2014; Vafai & Tien, 1989):

$$\rho C_p \frac{\partial T}{\partial t} + \rho C_p u_f \cdot \nabla T - \nabla \cdot (k \nabla T) = - \left(L_f {}^i \hat{e}^w + L_v {}^w \hat{e}^g \right) \quad (8)$$

The first term on LHS represents energy generation or consumption, and the second term on LHS denotes heat convection caused by water/vapor diffusion ($u_f = \varepsilon^w v^{w,s} + \varepsilon^v v^{v,s}$). The third term on LHS represents heat conduction, and the RHS term is the heat source/sink within the REV due to phase changes (freezing/melting and condensation/evaporation). These thermophysical properties also need to be represented in the heat transfer equation. For example, the specific heat capacity change can be calculated by the derivative of enthalpy with respect to temperature ($C_p(T) = dH(T)/dT$). The apparent specific heat shows a drastic reduction just below the initial freezing temperature, which indicates a major

removal of the latent heat of fusion from the material (Heldman, 1982). Thus, the latent heat effect can be approximated by using a large specific heat capacity over a small temperature range. This dramatic change within a small temperature range could produce discontinuity and cause computational difficulty in the simulations. Therefore, the transition temperature approximation is necessary for the model to account for the effect of latent heat on temperature variation in the energy equation. A transition temperature region ΔT around freezing temperature T_f during phase change was included with a smoothing variable, θ (Voller & Prakash, 1987). θ depends on the temperature with range of $T_f - \frac{\Delta T}{2} < T < T_f + \frac{\Delta T}{2}$. $\theta = 1$ represents the frozen state when $T \le T_f - \frac{\Delta T}{2}$; $\theta = 0$ represents the unfrozen state when $T \ge T_f + \frac{\Delta T}{2}$; while $0 < \theta < 1$ represents the transition zone (also termed as mushy zone in the phase change literature), when the temperature is between $T_f - \frac{\Delta T}{2} < T < T_f + \frac{\Delta T}{2}$. The density ρ and thermal conductivity k in Equation (8) can be obtained from the relations of mixture properties for frozen and unfrozen states, which are given as (Voller et al., 1990):

$$\begin{aligned} \rho &= \theta \rho_{phase1} + (1-\theta)\rho_{phase2}, \\ k &= \theta k_{phase1} + (1-\theta)k_{phase2} \end{aligned} \quad (9)$$

where phase 1 represents the frozen phase (*s, g, i, w*) and phase *2* represents the unfrozen phase (*s, g, w*).

The apparent heat capacity method is used to include the latent heat, which causes discontinuity of specific heat capacity near the freezing point. In the transition zone (Bonacina et al., 1973), a mass fraction α_m is defined as equal to $\frac{1}{2}$ when $T = T_f + \frac{\Delta T}{2}$, and $-\frac{1}{2}$ when $T = T_f - \frac{\Delta T}{2}$.

$$\alpha_m = \frac{1}{2} \frac{(1-\theta)\rho_{phase2} - \theta \rho_{phase1}}{\theta \rho_{phase1} + (1-\theta)\rho_{phase2}} \quad (10)$$

Enthalpy change due to phase change during freezing can be written as

$$h_{water} = h_{ice} + \int_{T_f - \Delta T/2}^{T_f + \Delta T/2} C_{pLH}(T)dT \quad (11)$$

C_{pLH} accounts for the specific heat capacity related to latent heat, which can be written as (Bonacina et al., 1973):

$$C_{pLH}(T) = L\frac{d\alpha_m}{dT} \quad (12)$$

The integral of the above quantity with T as the independent variable represents the latent heat release/gain during phase change (Bonacina et al., 1973):

$$\int_{T_f - \Delta T/2}^{T_f + \Delta T/2} C_{pLH}(T)dT = \int_{T_f - \Delta T/2}^{T_f + \Delta T/2} L\frac{d\alpha_m}{dT}dT$$

$$= LL[\alpha_m(T_f + \Delta T/2) - \alpha_m(T_f - \Delta T/2)]$$

$$= L\left[\frac{1}{2} - \left(-\frac{1}{2}\right)\right] = L \quad (13)$$

In the model, the specific heat of high moisture food was assumed to be dominated by water and ice fractions. Therefore, the apparent heat capacity can be written as:

$$C_p = \frac{1}{\rho}(\theta \rho_{phase1}C_{pi} + (1-\theta)\rho_{phase2}C_{pw}) + L\frac{\partial \alpha_m}{\partial T} \quad (14)$$

2.5 | Stress and strain during freezing

Foods undergo volume expansion during freezing due to the expansion of water, which subsequently leads to mechanical stresses in the biopolymeric matrix. Additionally, the mechanical properties change due to water loss caused by cooling air, the temperature dependence of properties, and phase transition. Deformation of the frozen material can be obtained from the displacement field. The linear momentum balance for an isotropic mixture of solids and fluids can be represented using Cauchy's first law of motion (Acheson, 1991):

$$\rho\frac{\partial^2 u}{\partial t^2} - \nabla_L \cdot \sigma = F_b \quad (15)$$

$u = u(X, Y, Z)$ is the displacement field, which defines the difference between the spatial (x) and material coordinates (X). The material coordinates are related to the original geometry and the spatial coordinates depend upon the deforming geometry. σ is the stress tensor, which is related to internal mechanical stresses in the biopolymers. F_b represents the body force and is ignored in this study as it small in comparison to the mechanical forces. The material time derivative of u provides the velocity of the solid frame (v^s). The solid matrix in a frozen food was assumed to be a linear elastic material. The mechanical stress was formulated as the sum of effective pore stress σ_p and elastic stress σ_E.

$$\sigma = \sigma_{p+}\sigma_E, \sigma_p = -P^{pore}I, \sigma_E = E\varepsilon \quad (16)$$

The pore pressure-based stress σ_p represents stress exerted by fluids on pore walls (Ehlers, 2002). The temperature-dependent deformation during freezing was estimated using the phase change strain calculated from the ratio of density of unfrozen matrix and frozen matrix.

By calculating the pore pressure, the effect of fluids' redistribution on the solid matrix can be understood, and the subsequent expansion or shrinkage in the biopolymeric matrix can be estimated (Ditudompo & Takhar, 2015; Netti et al., 2003). The pore pressure is expressed by $P^{pore} = s^w P^w + s^g P^g$, where s^w and s^g are the degrees of water and gas saturation (Ehlers, 2002). To capture the biomaterial expansion due to phase change during freezing, its contribution to total strain was calculated asl:

$$E = \frac{1}{2}[\nabla u + (\nabla u)^T],$$

$$E_{XX} = E_{YY} = E_{ZZ} = E_{elastic} + E_{phch},$$

$$E_{phch} = \frac{1}{3}\frac{dv_{frozen}}{dV_{unfrozen}} = \frac{1}{3}\frac{\rho_{unfrozen}}{\rho_{frozen}} \qquad (17)$$

where the deviatoric components of Lagrangian strain (E) were taken as zero due to the assumption of uniform dilatation. The elastic strain was calculated from the coefficient of elasticity and stress in the material. The density values for the frozen and unfrozen matrices were calculated using Equation (9).

2.6 | Species transport

In fruits and vegetables, solutes may be present in the form of sugars, salt, ascorbic acid, and so forth (Bradshaw & Bonierbale, 2010). As the ice crystals are formed in frozen foods, water migrates to the crystallization sites and changes to ice, accounting for a higher concentration of solutes in the remaining unfrozen region. The increase in solute concentration in the unfrozen areas causes their diffusion to dilute regions, where depression in freezing point occurs (Chen & Chen, 1996; Gabas et al., 2003). The freezing point depression is an essential characteristic of food materials (Chen et al., 1996).

The macroscale mass balance equation for the jth species (salt, sugar, vitamin C, etc.) in the fluid phase can be written as (Singh et al., 2003b):

$$\frac{D^s(\varepsilon^w \rho^{w_j})}{Dt} + \nabla \cdot (\varepsilon^w \rho^{w_j} v^{w_j,s}) - \frac{\varepsilon^w \rho^{w_j}}{\varepsilon^s}\frac{D^s \varepsilon^s}{Dt} = 0, \text{with } j$$
$$= 1 \cdots N \qquad (18)$$

where $v^{w_j,s}$ is given by

$$v^{w_j,s} = -D_j \nabla(\varepsilon^w \rho^{w_j}) \qquad (19)$$

where $\rho^{w_j} = m^j/V^w$ is the solute concentration or density in the fluid phase. Thus, $\varepsilon^w \rho^{w_j} = (V^w/V^{Total})(m^j/V^w) =$

m^j/V^{Total} represents the solute concentration in the macroscale food matrix.

3 | TRANSFORMING FROM EULERIAN TO LAGRANGIAN COORDINATES

During freezing, expansion or shrinkage occurs in frozen products because of the density differences between solid ice and liquid water. Therefore, the freezing process involves a moving boundary problem. All equations described above were transformed into the Lagrangian framework, where the solution was obtained using a stationary mesh. The solution was converted back to the Eulerian framework, as discussed under the solution methodology. In the porous material, the coordinate framework was tied to the solid material point for which the following relation holds (Singh et al., 2003b):

$$\varepsilon^s \rho^s j^s = \varepsilon_0^s \rho_0^s \qquad (20)$$

where j^s is the determinant of the Jacobian matrix. Since the solid phase in this study is assumed to be incompressible at the microscale ($\rho^s = \rho_0^s$), Equation (20) simplifies to $j^s = \varepsilon_0^s/\varepsilon^s$.

The volume deformation of the material is assumed to follow a uniform dilatation/shrinkage during freezing/thawing, due to which the differential length in three linear dimensions will follow $dx/dX = dy/dY = dz/dZ = \zeta$, which results in:

$$j^s = \zeta^3 \qquad (21)$$

The Eulerian gradient operator can be represented as:

$$\nabla_E \equiv \frac{\partial}{\partial x}\hat{e}_x + \frac{\partial}{\partial y}\hat{e}_y + \frac{\partial}{\partial z}\hat{e}_z \qquad (22)$$

For uniform dilation/shrinkage, the Eulerian and Lagrangian gradient operators are related using the chain rule as:

$$\nabla_E \equiv \frac{\partial X}{\partial x}\frac{\partial}{\partial X}\hat{e}_X + \frac{\partial Y}{\partial y}\frac{\partial}{\partial Y}\hat{e}_Y + \frac{\partial Z}{\partial z}\frac{\partial}{\partial Z}\hat{e}_Z$$
$$= \frac{\partial X}{\partial x}\left(\frac{\partial}{\partial X}\hat{e}_X + \frac{\partial}{\partial Y}\hat{e}_Y + \frac{\partial}{\partial Z}\hat{e}_Z\right) = \frac{1}{\zeta}\nabla_L \quad (23)$$

Thus, we obtain

$$\nabla_E = j^{s(-1/3)}\nabla_L = \left(\varepsilon_0^s/\varepsilon^s\right)^{-1/3}\nabla_L \qquad (24)$$

The Eulerian gradient operators in above Equations (3), (5)–(8), (10)–(13), (23), and (24) can be replaced with Lagrangian operators using the above relation.

4 | INPUT PARAMETERS AND MATERIAL PROPERTIES

The supplementary parameters and properties for solving this two-scale unsaturated transport model can be found in Table 1. Fruits and vegetables can exhibit anisotropic material properties. However, the properties were assumed to be isotropic in this study. The key relationships are discussed in detail below.

4.1 | Moisture content

The moisture content in the frozen foods includes both water and ice content. Therefore, the moisture content (g/g solids) can be calculated from the volume fraction of water and ice:

$$X_w = \frac{\varepsilon^w \rho^w + \varepsilon^i \rho^i}{\varepsilon^s \rho^s} \qquad (25)$$

4.2 | Phase change term

The phase changes are not instantaneous phenomena during evaporation between water and vapor or freezing between water and ice and are governed by the Gibbs free energy differences between different phases (Fang & Ward, 1999; Takhar, 2014). The phase change rates play a crucial role via the source/sink terms to couple the unsaturated mass balance equations of water, gas, and ice phases (Bansal et al., 2015). The mass exchange term arises during upscaling in macroscale equations derived using HMT (Bennethum & Cushman, 1996). Takhar (2014) states that when the system is near equilibrium, the mass exchange rate between α and β phases is directly proportional to their Gibbs free energy difference, which can be expressed by:

$$\xi^\beta \hat{e}^\alpha = G^\beta - G^\alpha = K\left(p^\beta - p^\alpha\right) \qquad (26)$$

where K is the constant of proportionality (Halder et al., 2007). While converting from Gibbs to pressure-based form, linearization of the pressure terms was performed (Fang & Ward, 1999). Therefore, the evaporation rate between liquid and gas can be represented using the following equation:

$$^w\hat{e}^g = {}^w\hat{e}^v = \xi^v\left(p_{eq}^v - p^v\right) \qquad (27)$$

where ξ^v is the evaporation rate constant, $p_{eq}^v = a_w p_{sat}$ is the equilibrium vapor pressure in the food matrix, a_w is the water activity, and p_{sat} is the saturated vapor pressure at a given temperature. The p^v is obtained from the ideal gas law: $p^v = \rho^v R^v T$, where the vapor density, ρ^v, is the dependent variable of Equation (4).

Differences in vapor pressure in frozen foods leads to water migration from unfrozen regions to frozen regions. The local vapor pressure difference between unfrozen and frozen surface can be utilized to calculate, the ice formation rate as:

$$^w\hat{e}^i = G^w - G^i = \xi^i\left(p_{eq}^v - p^i\right) \qquad (28)$$

ξ^i is the rate constant of freezing, which can be estimated by the reciprocal of freezing time. This parameter was estimated inversely during simulations. The parameter is not expected to be a constant, but due to lack of experimental information, it was assumed to be a constant. p^i is the partial vapor pressure in the immediate vicinity of the ice surface in the porous matrix.

4.3 | Freezing point depression

Conversion from water to ice causes an increase in solute concentration in the unfrozen region. The freezing point of the region with higher solute concentration is lower than that of the dilute region. This is also termed freezing point depression. Freezing point depression is a colligative property of matter and is directly proportional to the molality (moles of solute/liter of solvent) of the solution (Atkins & De Paula, 1998):

$$\Delta T_f = K_f m_b i \qquad (29)$$

where K_f is the freezing point depression constant and m_b is the molality of the solute. They are represented as:

$$K_f = R\frac{T_m^2}{\Delta H_f}, m_{solute} = \frac{\rho^{w_j}}{M_{solute}} \qquad (30)$$

Here i is the factor denoting the number of individual particles/ions for a substance in solution. For instance, $i = 1$ for sugar in water, and $i = 2$ for sodium chloride in water. m_{solute} is the molar concentration of solute (mole of solute per liter of water). ρ^{w_j} is kg of solute per liter of water, which is the dependent variable of Equation (23), and M_{solute} is molecular mass of the solute (kg of solute/mole of solute). The freezing temperature is defined as $T_f = T_{f0} - \Delta T_f$, which is coupled in the energy balance and mechanical equations. Assuming dilute concentration, m_b was taken equal to m_{solute}.

TABLE 1 Supplementary parameters and properties used for solution of the model

Parameters	Expression	Source
Coefficient of elasticity (Pa)	3.74×10^6	Finney and Hall (1967)
Density (kg/m³)		
Water	$838.466 + 1.401T - 3.011 \times 10^{-3}T^2 + 3.718 \times 10^{-7}T^3$	Poling et al. (2001)
Ice	$1032.46 - 1.39T + 6 \times 10^{-3}T^2 - 9.28 \times 10^{-6}T^3$	Fukusako (1990)
Solid (Biopolymers)	1240	Takhar (2014)
Diffusivity (m²/s)		
Water	$1.52 \times 10^{-7} \exp(-50/R_u T)$	Zogzas, et al. (1996)
Vapors	$0.049 \times (D_{ia})^2 / t_{1/2}$ with $t_{1/2} = 12000\,\text{s}$ for potato	Saravacos & Stinchfield (1965)
Solute	0.78×10^{-9}	Wollhöver et al. (1985)
Evaporation rate constant (s/m²)	0.3	(Zhao, 2019)
Ice formation rate constant (s/m²)	4×10^{-3}	(Zhao, 2019)
Latent heat of freezing (J/kg)	3.33×10^6	Fukusako (1990)
Latent heat of vaporization (J/kg)	$2.792 \times 10^6 - 160T - 3.43T^2$	Stanish et al. (1986)
Ice expansion coefficient (1/K)	$\alpha = 5.27 \times 10^{-5}$ when $T \leq 273.15\,\text{K}$	La Placa and Post (1960)
Mass transfer coefficient (m/s)	0.05	Estimated as per Ditudompo & Takhar (2015)
Permeability (m²)		
Water	$D^w \times \mu^w / E$	Takhar (2014)
Gas	$4.57 \times 10^{-11} \exp(-10.86 S^w)$	Feng et al. (2004)
Poisson's ratio	0.492	Finney & Hall (1967)
Saturated vapor pressure (Pa)	$p_{sat} = \exp[-6096T + 21.24 - 2.71 \times 10^{-2}T + 1.67 \times 10^{-5}T^2 + 2.434\ln(T)]$	Perry & Green (1997)
Specific heat (J/kg·K)		
Water	$12010.14 - 80.40T + 0.31T^2 -5.38 \times 10^{-4}T^3 + 3.62 \times 10^{-7}T^4$	Zábranský et al. (2001)
Ice	2108	Möller (2014)
Vapor	$13604.73 - 90.43T + 0.277T^2 -4.21 \times 10^{-4}T^3 + 3.18 \times 10^{-7}T^4 - 9.56 \times 10^{-11}T^5$	Poling et al. (2001)
Air	$1047.63 - 0.37T + 9.45 \times 10^{-4}T^2 -6.02 \times 10^{-7}T^3 + 1.28 \times 10^{-10}T^4$	Poling et al. (2001)
Thermal conductivity (W/(m·K))		
Water	0.613	Iyahraja & Rajadurai (2015)
Ice	2.4	Fukusako (1990)
Vapor	$1.317 \times 10^{-4} + 5.150 \times 10^{-5}T + 3.896 \times 10^{-8}T^2 - 1.368 \times 10^{-11}T^3$	Vargaftik (1975)
Air	$-2.276 \times 10^{-3} + 1.155 \times 10^{-4}T - 7.903 \times 10^{-8}T^2 +4.117 \times 10^{-11}T^3 - 7.439 \times 10^{-15}T^4$	Vargaftik (1975)
Gas mixture	$k^g = \frac{X^v k^v}{X^a \Phi^{va} + X^v} + \frac{X^a k^a}{X^v \Phi^{av} + X^a}$ where $X^v = P^v/P^g, X^a = 1 - X^v$ $\Phi^{\alpha\beta} = \frac{1}{\sqrt{8}}(1 + \frac{M^\alpha}{M^\beta})^{-1/2}[1 + (\frac{\mu^\alpha}{\mu^\beta})^{1/2}(\frac{M^\beta}{M^\alpha})^{1/4}]^2$ where $\alpha = a \beta = v$; or $\alpha = v, \beta = a$	Bird et al. (2002)

(Continues)

TABLE 1 (Continued)

Parameters	Expression	Source
Viscosity (Pa·s)		
Water	0.001	Baxter & West (1977)
Vapor	$1.42 \times 10^{-6} + 3.83 \times 10^{-8}T - 3.852 \times 10^{-12}T^2 + 2.101 \times 10^{-15}T^3$	Poling et al. (2001)
Air	$-8.38 \times 10^{-7} + 8.357 \times 10^{-8}T - 7.69 \times 10^{-11}T^2$ $+4.644 \times 10^{-14}T^3 - 1.06 \times 10^{-17}T^4$	Poling et al. (2001)
Gas mixture	$\mu^g = \frac{X^v \mu^v}{X^a \Phi^{va} + X^v} + \frac{X^a \mu^a}{X^v \Phi^{av} + X^a}$	Bird et al. (2002)
Water activity	$a_w = \frac{1}{1+0.0097T_f + CT_f^2}$ where $C = 5 \times 10^{-2}$	Chen (1987)
Universal gas constant (J/(K·mol))	$R = 8.314,$	Perry & Green (1997)

4.4 | Capillary pressure

In Equation (10), the water velocity is determined by the pressure gradient (∇P^w) and concentration gradient ($\nabla \varepsilon^w$) using the generalized Darcy's law relations. To calculate the water phase pressure P^w, the capillary pressure relation was used. It is given by (Grant & Sletten, 2002; Spolek & Plumb, 1981):

$$P^w = P^g - p^{cw}, \quad p^{cw} = 8.4 \times 10^4 s^{w^{-0.63}} \quad (31)$$

4.5 | Heat transfer coefficient

To calculate the heat transfer during freezing Neumann type of boundary condition was used:

$$Q_T = -h_c (T - T_{amb}) \quad (32)$$

where h_c is the heat transfer coefficient and T_{amb} is the freezer temperature.

The heat transfer coefficient around the frozen material can be determined using the Nusselt number-based correlations (Cengel et al., 1998).

$$h_c = \frac{Nu \, k_{fm}}{D_{ia}}$$

$$Nu = 0.683 \text{Re}^{0.466} Pr^{1/3}, with 40 < Re < 4000. \quad (33)$$

where k_{fm} is the thermal conductivity of the freezing medium, Re is Reynolds number, and Pr is the Prandtl number, which can be calculated by thermophysical properties such as density, heat capacity, and viscosity of the freezing medium.

5 | INITIAL AND BOUNDARY CONDITIONS

The initial moisture content (X_{wi} gram of water/gram of solid) of raw potato was measured experimentally. Initial gas volume fraction was taken as (ε_0^g) (Bansal et al., 2015). The initial volume fraction of water phase was obtained by the following relation:

$$\varepsilon_0^w = \frac{X_{wi}\rho_0^s(1 - \varepsilon_0^g)}{X_{wi}\rho_0^s + \rho_0^w} \quad (34)$$

The initial ice volume fraction ε_0^i was assumed to be 0, which means no ice was present at the beginning of a simulation. The initial volume fraction of solid polymer was calculated from:

$$\varepsilon_0^s = 1 - \varepsilon_0^g - \varepsilon_0^w - \varepsilon_0^i \quad (35)$$

Therefore, the initial conditions for fluid and ice transport equations were:

$$\varepsilon_0^w = 0.85, \varepsilon_0^i = 0, \varepsilon_0^g = 0.03, \varepsilon_0^s = 1 - \varepsilon_0^g - \varepsilon_0^w = 0.12 \quad (36)$$

For the gas and vapor equations, initial pressure inside the material was assumed to be equivalent to the atmosphere pressure:

$$P_i = P_{atm} \quad (37)$$

For energy balance, the initial temperature of the material was set at $T_i = 278.15K(5°C)$ as the start point for the freezing simulation.

For the solute transport equation, the potato solute concentration was taken as 0.1 M, which is of the order of magnitude for potatoes solute concentration given by (Bartolome & Hoff, 1972). The product of this solute

concentration and molecular mass of sodium chloride is the initial solute density $\rho_0^{w_j}$:

$$\rho_0^{w_j} = m_{solute} M_{salt} = 0.1\,[\text{mol/L}] \times 58.44\,[\text{g/mol}]$$

$$= 5.844\,[\text{g/L}] = 5.844\,[\text{kg/m}^3] \tag{38}$$

The Neumann boundary conditions were utilized for the various transport equations as follows. For the water and vapor transport (Equations 1 and 4), the boundary conditions were:

$$Q_w = -h_m(\rho_{eq}^v - \rho_{amb}^v) \tag{39}$$

$$Q_v = -h_m(\rho^v - \rho_{amb}^v) \tag{40}$$

For gas transport and mechanical equations (Equations 3 and 15), the gas pressure at the boundary was considered to be equivalent to the atmospheric pressure ($P_{surface}^g = P_{atm}$). For the ice phase and solute transport equations (Equations 2 and 18), it was assumed that the material was isolated, and there was no exchange of ice or solute from the atmosphere to inside. Therefore, the following no-flux boundary conditions were used: $Q_i = 0$ and $Q_{w_j} = 0$. Various parameters and properties needed for obtaining the solution are given in Table 1.

6 | SOLUTION OF MATHEMATICAL MODEL

6.1 | Problem description

Figure 1 illustrates the physical transport mechanisms occurring in a French fry-shaped potato during freezing. The potato is comprised of solid, water, ice, and vapor phases. The solid phase contains biopolymers and builds the geometry frame. The moisture inside the material can exist in the form of liquid water, ice, and water vapors depending upon different conditions. Water, vapors, and air are considered as compressible fluid phases that can diffuse and migrate during the freezing process. At the beginning of freezing, the temperature inside the sample decreases from its initial temperature to the phase change point, which is called the precooling stage (Zhao & Takhar, 2017a). During this stage, the process is similar to a drying phenomenon since no ice is formed. Water may migrate and transfer to vapor near the surface due to the partial pressure difference between water and the surrounding air (Takhar, 2014). When the temperature inside the sample reaches its freezing point, the nucleation begins, and phase change starts. As water changes to ice, the solute concen-
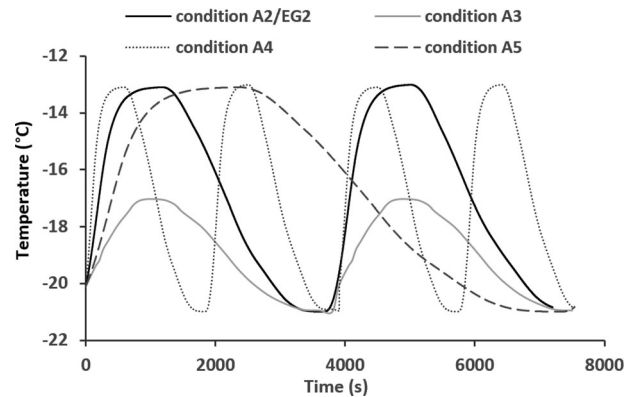

FIGURE 2 Fluctuating freezing medium temperature profiles plotted as a function of time

tration increases in the unfrozen regions and depresses the freezing point. While a large amount of latent heat is released during phase change, the temperature may not drop dramatically, which is called a freezing plateau (Zhao & Takhar, 2017a). After this plateau, the temperature continues to decrease to approach the ambient temperature in the freezer (T_{amb}).

6.2 | Modeling conditions

The HMT-based multiscale transport model integrates the multiscale transport mechanisms of mass, momentum, species, and energy during the freezing process. Table 2 and Figure 2 depict the ambient temperature profiles (T_{amb}) as a function of simulated time, which were utilized for the energy balance equation's boundary condition (Equation 32). The temperature variations, frequencies, and cooling type in the freezer are considered in the simulation setting to achieve an understanding regarding the mass and heat transfer into biopolymers during the freezing process.

6.3 | Materials and methods

Russet brown variety of potatoes (*Solanum tuberosum*) (Potatoes Goodness Unearthed®, United States Potato Board Inc., CO, USA) were purchased from a local grocery store (Walmart Supercenter, Pullman, WA, USA). The potatoes were stored in a cold room for 24 h to keep their initial temperature around 5°C. The initial moisture content of potatoes was measured using the oven-dry method with air temperature of 105°C for 24 h (Reeb et al., 1999).

The potatoes were cut into rectangular sizes (2 cm × 2 cm × 6 cm), which was also the geometry used for solving the model. The cut samples were wrapped using flexible plastic film (Glad® Cling Wrap, The Glad Products

TABLE 2 Different freezing temperatures applied as the boundary conditions for the energy transport equation (Equation 21)

Conditions	Ambient temperature in the freezer	Frequency	Freezing medium	Application
Condition EG1	Constant: −21°C	Normal	Ethylene glycol	For model validation
Condition EG2	Fluctuated: −21 to −13°C	Normal		
Condition A1	Constant: −21°C	Normal	Air	Different magnitude of fluctuating temperature
Condition A2	Fluctuated: −21 to −13°C	Normal		
Condition A3	Fluctuated: −21 to −17°C	Normal		
Condition A4	Fluctuated: −21 to −13°C	Double	Air	Different frequency of fluctuating temperature
Condition A5	Fluctuated: −21 to −13°C	Half		
Condition A6	Open–close: 600 to 660s	Normal	Air	Sudden temperature rise imitating opening and closing of freezing cabinet door
Condition A7	Open–close: 6600 to 6660 s	Normal		
Condition A8	Multiple opening and closing of door: 6000 to 6060 s, 6300 to 6360 s, 6600 to 6660 s, and 6900 to 6960 s	Normal		

Company, Oakland, CA, USA) and put in a freezer, which used an aqueous solution of 50% ethylene glycol as the cooling agent (VWR Scientific, Arlington Heights, IL, USA). One potato sample was placed in the center of the bath, at a time. All faces of the potato sample received equal liquid flow—the potato sample was submerged in the ethylene glycol bath suitably to ensure that it was exposed uniformly to fluid flow.

Since the study involved solving a complex transport model for elucidating mechanisms in a complex food material, the ethylene glycol-based liquid cooling method was utilized, as it allowed changing the external temperature rapidly and with greater control. Once the physics being described by model was validated, it was utilized to conduct simulations with air cooling by changing the appropriate boundary conditions.

Two types of validation conditions were selected. The first type utilized an ethylene glycol bath maintained at −21°C (denoted as condition EG1). The second type of condition required fluctuating the temperature inside the ethylene glycol bath (denoted as condition EG2). At the start of a fluctuating temperature experiment, the bath temperature was reduced to −21°C. Then, the bath set temperature was changed to −13°C. In this manner, the ethylene glycol bath temperature fluctuated between −21°C and −13°C. The trend is plotted in Figure 2. The ethylene glycol temperature was used as T_{amb} for the heat transfer boundary condition (Equation 32). The core temperature of the potato and the freezer's temperature were recorded and monitored per second using external K-type

thermocouples (Omega Engineering Inc., Norwalk, CT) for 2 h. The temperature profiles were recorded using a data logger (Hioki LR8431-20 PRO, Hioki USA Corporation, Cranbury, NJ) for the required time as per the experiment.

A thin K-type thermocouple of diameter 0.05–0.81 mm was used to measure the transient temperatures at the geometric center of potato sample of 2 cm × 2 cm × 6 cm. Thin wire thermocouple is expected to have negligible influence on the accuracy of temperature measurement of the sample. Though we used a lab-scale freezing unit, the temperature fluctuation of 8°C was based on average temperature cycling most products experience during commercial storage and transport situation.

6.3.1 | Measurement of initial freezing point

The initial freezing point of the potatoes was determined using a Differential Scanning Calorimeter (DSC, Q2000 V24.10, TA Instruments, New Castle, DE). Commercially dried potatoes (Oregon Potato Co., Boardman, OR) were hydrated with a precalculated amount of water to obtain the varying moisture contents of 75%, 70%, 65%, 60%, and 55% on wet basis. For each moisture content measurement, 15 ± 2 mg of a sample was equilibrated at 25°C for 1 min, cooled to −25°C at the rate of 5°C/min, held isothermally for 5 min and then heated to 25°C at a rate of 5°C/min. The initial freezing points (T_f) were detected from DSC thermograms, which were −1.1°C, −1.3°C, −1.3°C, −1.3°C, and −1.7°C for potatoes with different initial moisture content
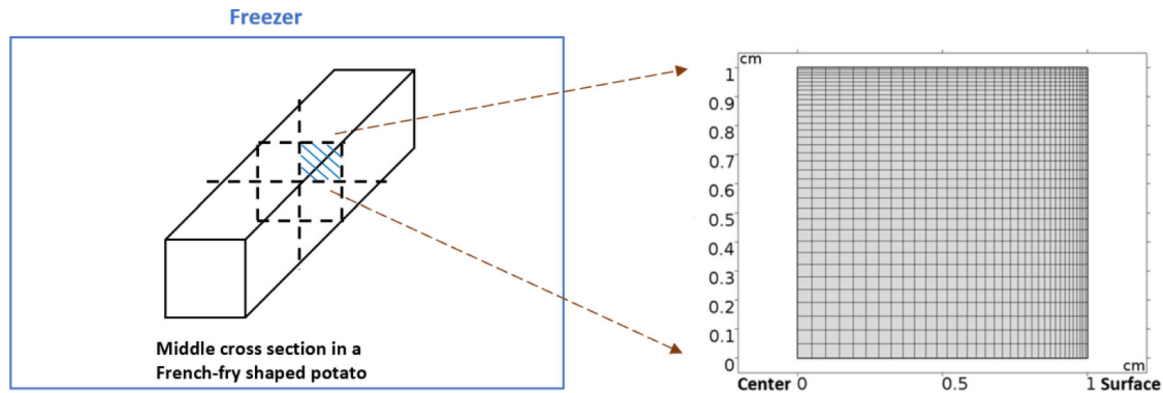
FIGURE 3 Schematic diagram of a French-fry-shaped potato used for solving the model. The French-fry-shaped potato was assumed to be placed in the middle of a freezer, free of touching any surrounding solid objects (the left figure's dimension is not to scale)

levels of 75%, 70%, 65%, 60%, and 55%, respectively (Kumar et al., 2018).

Differential scanning calorimetry (DSC) is most reliable technique for measurement of initial freezing point of food products. Since the initial freezing point of food products depends on the chemical composition especially water content of the product, DSC was used to determine the initial freezing point of potato samples used in this study.

6.4 | Numerical solution and model validation (RMSE)

The frozen material was assumed to be of a cuboidal shape resembling French fries, with significantly longer initial length (6 cm) than its height (2 cm) and width (2 cm). Therefore, a 2D finite element geometry was used during simulations. Due to the symmetric shape and boundary conditions, one-quarter of the cross section was meshed to save computational time (Figure 3). Governing equations were solved using a commercial finite elements software package (COMSOL Multiphysics Ver 5.3a; Comsol, Burlington, MA, USA). The computation domain was 1 cm × 1 cm with the mapped mesh containing 1225 quadrilateral elements. The predefined distribution ratio for the elements was set as 7, which creates finer mesh near the surface to increase the solution accuracy in the regions expected to have larger gradients of various variables. The solution was achieved using the MUMPS solver with a free time step size of 1 s and maximum time-step of 5 s. Each simulation run took 25 to 120 min on a PC with Intel Core i7 processor with 2.2 GHz and 16 GB RAM. The simulation time depended upon whether the boundary conditions were of constant or fluctuating type, with the latter requiring more time to solve.

The dependent variables ε^w, ε^i, ε^g, and ε^s were solved to understand the interactions between the water, ice, gas,

and solid biopolymer phases. To validate the model, simulation results were compared to the experimental data using the root mean square error (RMSE):

$$RMSE = \sqrt{\sum_{i=1}^{n}\left(X_{\exp} - X_{pred}\right)^2 / n} \quad (41)$$

where n is the number of data points ($n = 3000$ for the constant freezing condition and $n = 7200$ for the fluctuating freezing condition), $X_{\exp}$ is the experimental data, and X_{pred} is the predicted value obtained from the model.

The experimental transient temperature profile at the product's geometric center was used to validate mathematical model developed under constant and fluctuating freezer temperature. Potato's geometric center and the freezer's temperature were recorded every second using external K-type thermocouples.

6.5 | Sensitivity analysis

Sensitivity analysis of critical thermo-physical properties was performed to better understand and explain the physical phenomena during the freezing process. The heat transfer coefficient (h_c in Equation 32) was tested between 250 W/(m² K) to 3500 W/(m² K) range (Figure 4). When h_c was greater than 1000 W/(m²·K) (liquid cooling), there was no significant difference for the center temperature profile. The center temperature was significantly different for $h_c < 250$ W/(m²·K) than higher h_c values, the regime in which air cooling is expected to lie.

The sensitivity analysis was also performed for the evaporation rate ξ^v, ice formation rate ξ^i, water diffusivity D^w, vapor diffusivity D^v, solute diffusivity D^j, mass transfer coefficient h_m, and gas permeability K_g. These parameters/properties were varied by ± 10% during simulations.
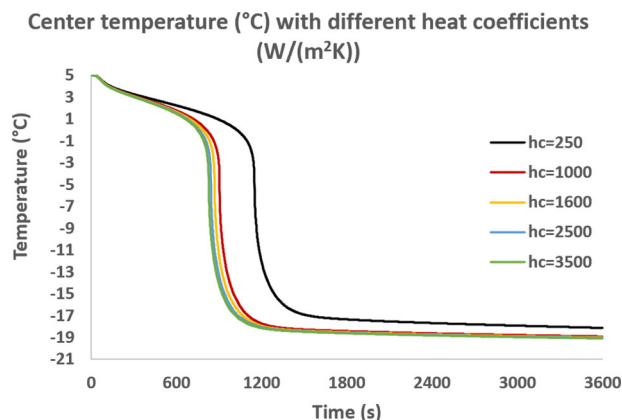
FIGURE 4 The center temperature profiles with different heat transfer coefficients for a constant $-20°C$, 1 h freezing
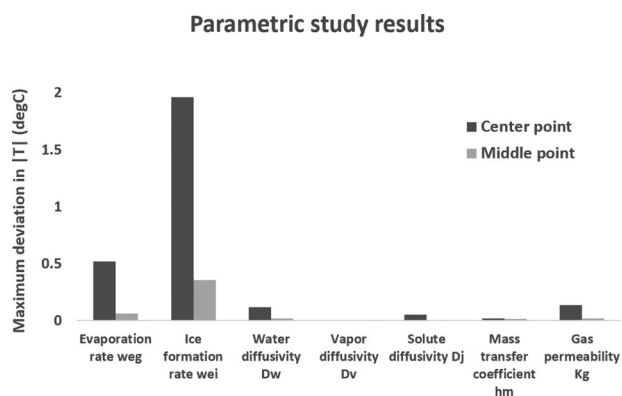

FIGURE 5 The effect of $\pm 10\%$ variation in a parameter on maximum deviation observed on product temperature

Figure 5 shows the maximum deviation in the center and middle point ($x = 0.5$ cm, $y = 0.5$ cm in Figure 3) temperature profiles for these sensitivity tests.

The evaporation rate ξ^v and ice formation rate ξ^i were more critical in affecting the center and middle point temperature in comparison to various other parameters (Figure 5). These phase-change rates are the source/sink terms for the mass balance equations and affect the local heat release/absorption (source/sink term) during freezing/melting. Especially the ice formation rate had the highest effect on the center temperature.

The water diffusivity, solute diffusivity, and gas permeability also influenced the simulations shown in Figure 5. The water and solute diffusivity are related to the water and solute diffusion rates, while the gas permeability can affect the gas and pore pressure during the freezing. The vapor diffusivity and mass transfer coefficient had no significant effect on the center and middle point temperature (Figure 5).

7 | RESULTS AND DISCUSSION

7.1 | Mesh independency study

A mesh independence study was conducted to check the convergence of numerical simulations. The effect of 100, 400, 1225, and 2500 mapped mesh elements on the center temperature profile was compared. A constant $-21°C$ freezing condition was used for this test. Only mesh size of 100 elements had significantly different temperature profiles. The remaining number of elements resulted in a similar center temperature profile. Therefore, 1225 elements were used as the optimum mesh size, as these would result in more accurate numerical calculation than 100 and 400 element mesh and save computation time in comparison to 2500 elements.

7.2 | Validation of model predictions

The predicted temperature profiles were validated using the experimental data for constant (condition EG1) and fluctuating freezing conditions (condition EG2) in an ethylene glycol-based freezer (Table 2). During preliminary trials, it was observed that there was no significant difference in temperature profiles due to width of the transition zone (ΔT) taken as 2°C or 5°C. Therefore, the width of the transition zone (ΔT) was taken as 2°C for all simulations. Instead of using a step function, the use of this transition zone temperature to transition the specific heat values from water to ice or vice versa helped to enhance numerical stability in the solution.

Figure 6 shows the comparison of predicted and experimental center temperature profiles for EG1 and EG2 conditions. The predicted temperature decreased from the initial temperature (5°C) to near freezing point during the precooling stage. When the center temperature reached the freezing point, ice started to form and a large amount of latent heat was released. Since the change in the apparent specific heat of the material transitioning from the liquid to frozen state was captured in this model, the decrease in center temperature slowed down and showed a plateau similar to the one discussed in Zhao and Takhar (2017b). The experimental results also showed similar trends to the predicted curve for both constant and fluctuating freezer temperatures. The predicted temperature profile dropped slightly faster than the experimental data (Figure 6). The lack of accurate information on the thermo-physical properties such as fluid diffusivity in the food material and heat transfer coefficient for the freezing medium could have caused the difference between the predicted and observed temperature data (Zorrilla & Rubiolo, 2005). Despite these uncertainties, the model predicted the temperature profile
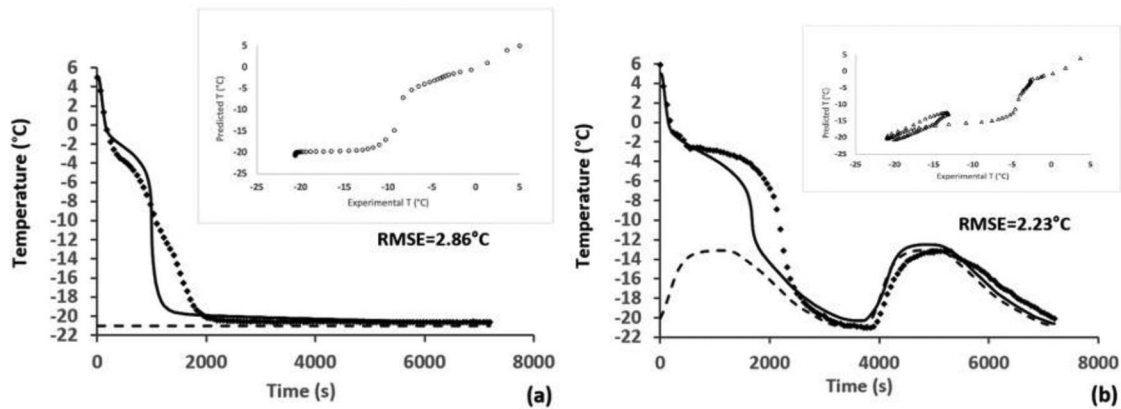
FIGURE 6 Validation of temperature predictions at the product's geometric center at (a) constant freezer temperature (Condition EG1 of Table 1) and (b) fluctuating freezer temperature (Condition EG2 of Table 1). In the main figure: the solid line (predicted data), symbols (experimental data), dashed line (ambient temperature). Inset figures show predicted versus experimental data

for constant and fluctuating freezing conditions with reasonable accuracy. The RMSEs between the predicted and experimental observations for conditions EG1 and EG2 are 2.86°C (for data up to 3000 s) and 2.23°C (for data up to 7200 s), respectively.

7.3 | Solute migration and freezing point depression

Species macroscale mass balance equations were used to calculate the solute transport in the frozen matrix. Predicted solute concentration was coupled with physical chemistry-based relation to calculate the freezing point depression in the food matrix. The calculated freezing point was utilized in the energy equation, which further affects the heat transfer, ice formation, and water diffusion. Figure 7 represents the predicted results for the freezing point as a function of unfrozen water content and the measured data. In some previous modeling studies with foods, the freezing point depression was ignored to obtain the solution in an easier manner (Poon & Peters, 2013). However, foods are complex biomaterials and mixtures of many ingredients. Water in food transfers to ice during freezing, leaving behind a solution whose concentration increases during the process. The increasing solute concentration contributes to the decrease in freezing point in the remaining unfrozen liquid. The lower freezing point would affect ice formation, water diffusion, and various interactions in foods during freezing (Newman & Wilson, 1997; Pham, 2008). In some previous studies, freezing point depression was estimated using the empirical equation for the aqueous solution (Chen, 1986; Chen & Chen, 1996). However, the empirical equations could not explain the freezing point variation in a real food material. In Figure 7, Chen's equation was fitted to the measured freezing point data (Kumar et al., 2018). The freezing point predicted by
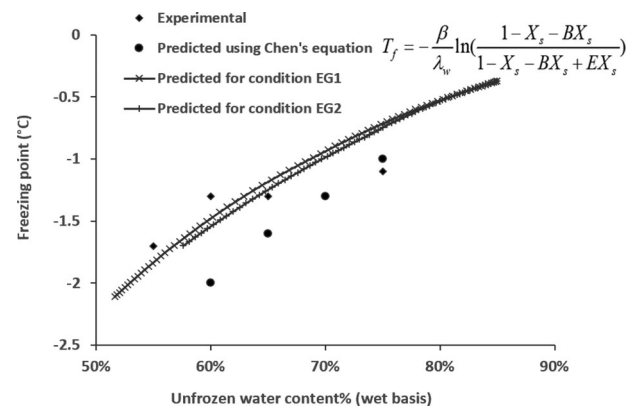

FIGURE 7 Comparison of predicted freezing point at a constant freezing medium temperature (solid line with cross marks) and at fluctuating medium temperature (solid line with vertical marks), experimental freezing point (diamond symbol), and data predicted using Chen's equation (circle symbol) (Chen, 1986; Chen and Chen, 1996)

the transport model presented in our study shows a better prediction of the experimental results than the empirical equation of Chen (Chen, 1986; Chen & Chen, 1996), especially in the regions of unfrozen water (Figure 7). Additionally, the numerical results for constant and fluctuating freezing conditions show a coherent prediction in the freezing point as a function of unfrozen water content. This indicates that transport equations coupled with physical chemistry-based relations utilized in this study are reliable in predicting the experimental freezing point data.

To analyze solute diffusion, the *x*-component water and solute velocity were plotted (Figure 8a,b). When freezing occurs near the surface and gradually moves toward the center, the unfrozen water movement is dominated by the fluid concentration and pressure gradient (Equation 6).
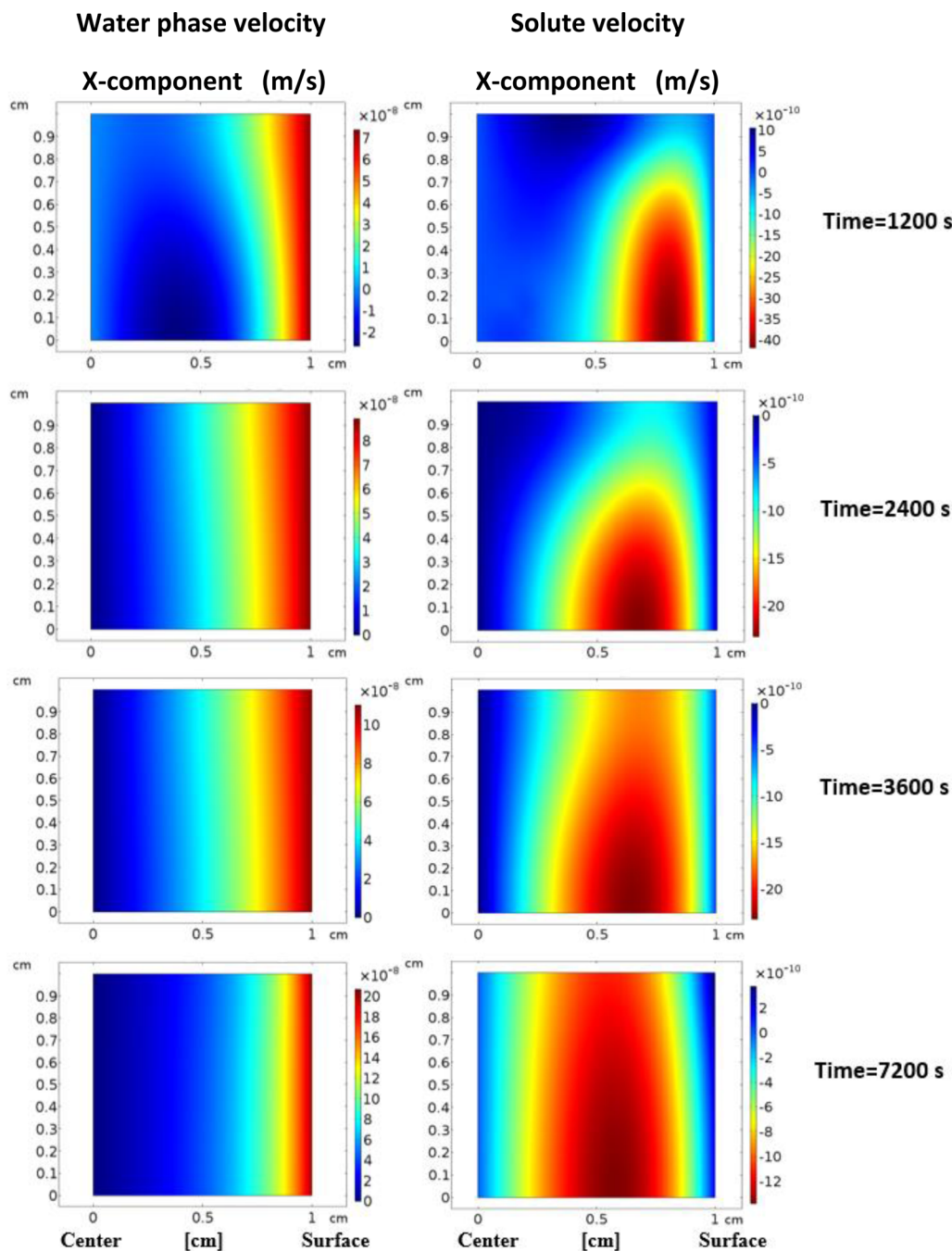
FIGURE 8 Magnitude of the *x*-component of unfrozen water (a) and solute velocity, (b) at different freezing times, represented on a surface plot of the cross-section in a French-fry-shaped potato for a constant freezing condition (−21°C). Positive magnitude denotes the flux direction toward +ve x axis from center to surface and vice versa

Water begins to move toward the frozen region near the surface from the center, which is indicated by the positive magnitude of water velocity (Figure 8a). The water also flows at a higher rate near the surface, where freezing happens first. Meanwhile, the frozen region's solute tends to be concentrated due to the lowering of moisture content, which produces a concentration gradient toward the center. This results in solute migration toward the center (Figure 8b). In Figure 8b, the negative magnitude of solute

velocity shows that solute is migrating from the frozen region (near the surface) toward the unfrozen region (near the center). The regions near the surface (which encounter heat removal earlier) have a higher rate of solute flux at 1200 s. As freezing progresses, the higher rate region shifts inward as the solute concentration shifts toward the center. When the temperature keeps dropping and ice keeps forming, the solute mobility is impeded, and the magnitude of solute flux is reduced. This results in the final solute

TABLE 3 Heat transfer parameters for air and Ethylene glycol freezing media

Heat transfer parameters	Air blast freezer	Ethylene glycol freezer
Density (kg/m^3)	1.20–1.25[a]	1100 (Usri et al., 2015)
Specific heat (J/[kg K])	1.9×10^3 (Andreas, 2005)	3266 (Chiam et al., 2017)
Dynamic viscosity (Pa·s)	1.6–1.7×10^{-5}[a]	2.2×10^{-3} (Chiam et al., 2017)
Thermal conductivity (W/[mK])	0.022–0.025[a]	0.258 (Selvam et al., 2017)
Velocity (m/s)	11 (Dempsey & Bansal, 2012)	2.6[b]
Surface heat transfer coefficient (W/(m^{2}K))	79–84[a]	2245[a]

[a]Calculated from expression defined in the Table 1.

[b]Data obtained from ethylene glycol freezer manufacturer.

concentration to be 12% higher near the surface than the center. To our knowledge, this is the first study utilizing the two-scale species transport equation coupled with the physical chemistry-based to predict the water and solute movement in a complex food material.

7.4 | Application results

After the model was validated using the experimental results in the previous section, it was used to perform real-world simulations discussed in this section. First, several variables (product temperature and volume fraction of various phases) for potatoes frozen using air (denoted as A) and ethylene glycol-based liquid (denoted as EG) freezing media are presented. As noted above, ethylene glycol was used in this study to validate the transport model and elucidate the transport mechanisms. Practical applications presented in this manuscript are focusing on air freezing, which is the commonly used freezing method in the food industry. When ethylene glycol-based liquid is used for cooling, the product temperature drops quickly over a small period of time (Peyghambarzadeh et al., 2011), which makes it easier to utilize this freezing method to test a complex freezing model such as the one presented in our manuscript. Ethylene glycol is an antifreeze that has a low freezing point (60% ethylene glycol aqueous solution's freezing point is about −46°C; Conrad et al. 1940) and provides a significantly higher surface heat transfer coefficient than air cooling (Table 3). Next, the effects of fluctuating freezing temperature at different amplitudes and frequencies, and intermittent freezing conditions caused by opening and closing of freezer doors are discussed.

7.4.1 | Comparison of air- and liquid-based freezing methods

Air blast freezing is a commonly used method in the frozen food industry that utilizes fans to circulate cold air through the freezer. Simulations with the model measured the amount of ice and unfrozen water content in the material, while in some previous modeling studies these amounts were estimated using a modified empirical function of temperature (Le-Bail et al., 2008; Rouaud & Pham, 2012). Figure 9 shows the ice and unfrozen water volume fraction distribution across the cross-section of a frozen potato at different times for a constant freezing medium temperature of −21°C. For condition EG1, ice started to form at the center after 300 s. For air freezing (condition A1) ice did not begin to form at the center until 900 s (Figure 9a,b). The ice volume fraction for condition EG1 had a higher magnitude than that for condition A1 at each time. The samples exposed to the air-based freezing method also showed an uneven ice distribution during freezing. The water volume fraction for both EG1 and A1 showed spatially homogeneous at X-component before 4800 s (Figure 9c,d), since the unfrozen water keeps moving during freezing. The unfrozen water movement is dominated by the fluid concentration and pressure gradient (Equation 6). Near the surface, more ice formed which resulted in a negative concentration and pressure gradient, so the water also flowed at a higher rate to offset the water transition to the ice. After 4800 s, the permeability and diffusivity of water became smaller because of the low temperature inside the material, which impeded the center water flowed to the surface, so the center had a higher unfrozen water volume compared to the surface one.

The amount of unfrozen water was observed to decrease more rapidly for condition EG1 compared to condition A1 before 1200 s (Figure 9c,d). Afterwards, however, the water volume fraction left in the EG1 sample is more than that for A1. Therefore, both unfrozen water and ice content for the air blast freezer are lower in comparison to the ethylene glycol freezer. The water's diffusivity and permeability based on different freezing media can also explain these predicted results. Newman and Wilson (1997) reported that the diffusivity and permeability of water are directly proportional to temperature but inversely proportional to ice content. Since the temperature slowly decreases in the sample stored in the air blast freezer, the diffusion coefficient and permeability of water would
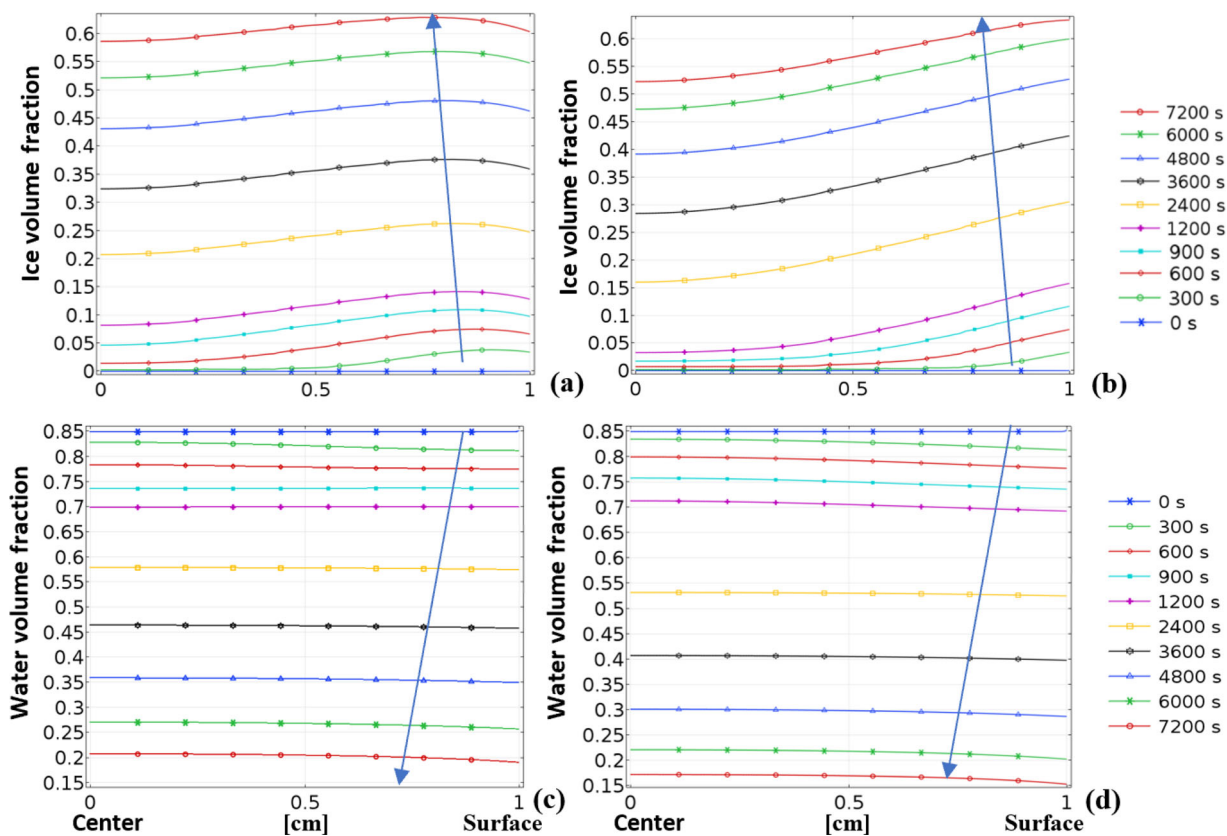
FIGURE 9 Predicted volume fraction distribution from the center to surface for the constant freezing condition (−21°C): (a) ice volume fraction for condition EG1. (b) Ice volume fraction for condition A1. (c) Water volume fraction for condition EG1. (d) Water volume fraction for condition A1

stay at a relatively higher value for a longer time, which results in a comparatively higher rate of water loss and lower rate of ice formation compared to the liquid-based freezer.

7.4.2 | Different fluctuating temperature cycle conditions

Since air blast freezing is a widely used method in the frozen food industry, this section aims to explore the modeling application of different fluctuating cycles (amplitudes or frequencies). Figure 2 illustrates different fluctuating temperature conditions that were applied as the boundary condition for the energy equation (Equation 8) in this study. Conditions A1 and A2 were the same as the freezer temperature used for the validation experiments. Condition A3 was the freezer temperature that follows the fluctuating trend as A2 but had a smaller varying magnitude between −21°C to −17°C. Condition A4 was the double frequency condition, with temperature changing between −21°C to −13°C four times during a simulation. Condition A5 represents the half frequency condition, with temperature only decreasing from −21°C to −13°C in 2 h.

7.4.3 | Deformation

The deformation ratio was also influenced by the fluctuating magnitude of the ambient freezing temperature. As it is well known, pure water expands by approximately 9% when it freezes because ice is less dense than the liquid water (Manga & Wang, 2007). However, since the food material is porous and includes multiple components, its volume deformation during freezing is more complicated than that of a pure substance.

The deformation of the food geometry was captured by calculating the effective pore pressure exerted by various fluids on the surrounding solid matrix and the strain due to phase change. The strain due to phase change causes a shift in mesh, which poses a challenge for the finite element simulations. However, since Eulerian-Lagrangian transformation was used in this study, this strain could be calculated during postprocess conversion of Lagrangian mesh to Eulerian mesh. Figure 10 depicts the linear strain (one-third of volumetric strain) calculated at −21°C for 4 h of drying at three points from center toward surface. During the precooling stage, the surface water would evaporate to surrounding air since the product surface was warmer than the ambient medium in the freezer (Pham, 2008).
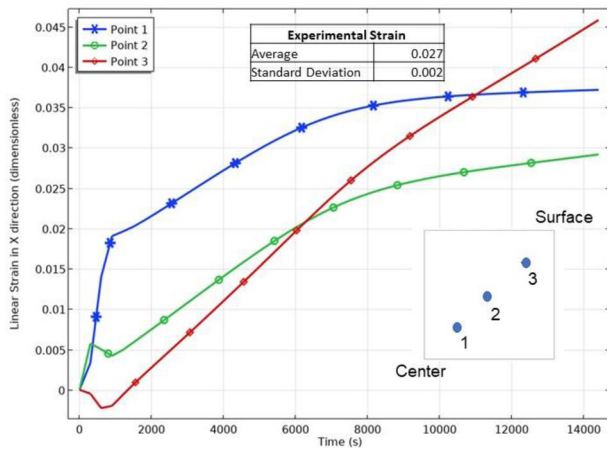
FIGURE 10 Calculated results for linear strain and its comparison to experimental strain at −21°C

Based on Equation (31), the lower water volume fraction gives rise to capillary pressure, and the high capillary pressure can cause negative gage water pressure (less than atmospheric) as the unfrozen water fraction decreases during freezing (Figure 11a,b). The pore pressure, which is the effective fluid pressure on the solid walls, was also reduced and became smaller than the atmospheric pressure (Figure 11c). This indicated that the pore structure in the material would be compressed, resulting in geometry shrinkage. Therefore, the strain becomes negative initially at Point 3 (Figure 10). In Point 2, the pore pressure causes a change in slope in the beginning (Figure 10). The negative gage pore pressure is caused by the water loss during the precooling stage. The negative pore pressure in porous matrices implies the ability of a porous matrix to hold moisture in unsaturated media (not saturated by liquid) and to suck fluid by capillary action when surrounded by the liquid medium. If the ice formation does not occur, the sample structure will keep shrinking, similar to a drying scenario. When the sample underwent phase change below its freezing point, the volume increased and caused a positive linear strain. There is an interesting trend shown in Figure 10. The point toward the surface had the maximum amount of freezing due to its vicinity toward the freezing medium. Therefore, this point showed maximum strain by the end of freezing time. However, this point also loses moisture faster. The center had a high amount of continuous strain change, as it had the highest amount of moisture. The middle point (Point 2) showed intermediate values between the two curves. We also conducted experiments to measure the strain in the potatoes and found the calculated strain in the same range as experimental values (see table inset in Figure 10). The strain values in a similar range were measured by McKellar et al. (2009) for potatoes frozen at −17°C.

Figure 11d shows the total stress calculated from pore pressure and thermal strain for the constant freezing condition A1. At 1200 s, as the sample's temperature dropped below its freezing point, phase change strain became dominant, and the total stress started to increase. After 3600 s, the material almost reached the set freezing temperature (−21°C), so the total stress did not increase significantly and resulted in a steady volume expansion.

7.4.4 | Simulation results for freeze–thaw cycle magnitudes of A1, A2, and A3

Figure 12 shows the distribution of ice volume fraction as a function of time at different spatial locations inside the material. The temperature fluctuation in a wider range (−21°C to −13°C) resulted in lower ice content, which can be observed from the result showing the ice volume fraction for condition A2 being smaller than condition A3. Both fluctuating air temperature conditions showed lower ice fraction than the constant air temperature condition A1. For example, at 7200 s, the center ice volume fraction is 0.55, 0.5, and 0.45 for constant freezing at −21°C, and the fluctuating temperature conditions of −21°C to −17°C, and −21°C to −13°C, respectively.

Additionally, the larger magnitude of fluctuating temperature generated more gas/vapor inside the material. The gas was less uniformly distributed in the sample during freezing and could contribute to uneven pore size inside frozen foods (Figure 13). As discussed in Zhao and Takhar (2017b), frozen products subjected to larger amplitude of freeze–thaw cycles caused larger average pore size and broader pore size distribution, as indicated by micro-computed tomography and image analysis. The simulation results for gas volume fraction correspond to this observation, as gas occupies the pore volume. For example, at 7200 s, the gas volume fraction was 0.19, 0.22, and 0.25 for constant (−21°C), −21°C to −17°C, and −21°C to −13°C, respectively. This was expected as the temperature fluctuation reduces ice formation, and the higher peak value of fluctuating temperature was prone to cause more water loss, which left more vapor and larger void in the interior of the frozen potato.

The higher gas content also implied more weight loss for the final product, since the vapor tends to flow through pores and leave the material during defrosting (Farid, 2002; Saravacos, 1967). The total moisture loss was 1.8%, 4.3%, and 4.7% for constant freezing at −21°C, fluctuating from −21°C to −17°C, and from −21°C to −13°C, respectively. Larger magnitudes of fluctuation caused more weight loss and produced more gas content, which is expected to create large pores. To prevent surface layer melting, the food
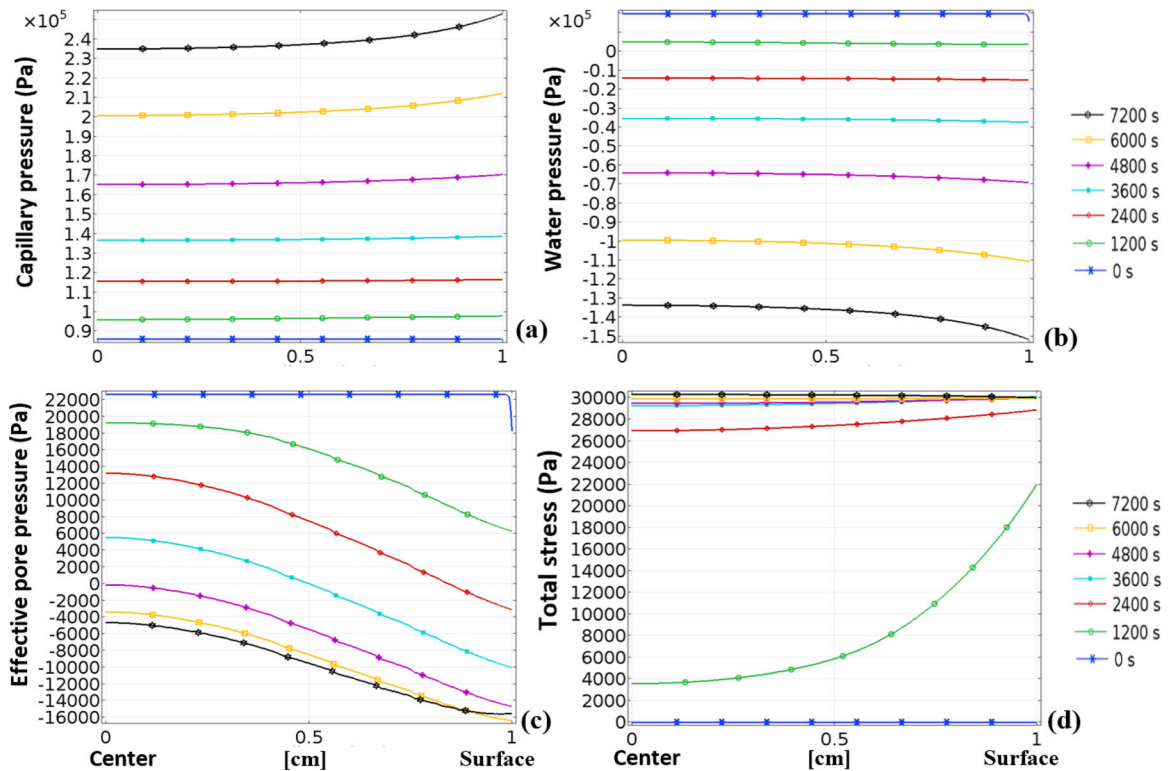
FIGURE 11 Spatial distributions of (a) capillary, (b) water, (c) effective pore pressure, and (d) total stress from the center to surface for constant freezing at −21°C
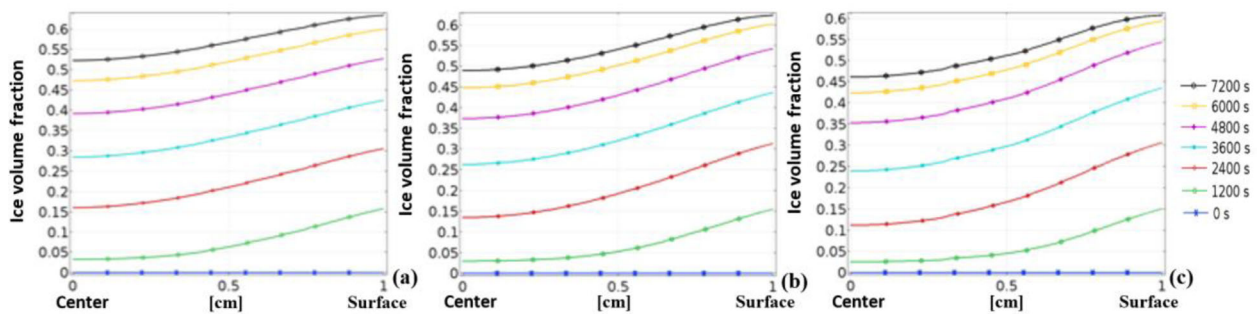

FIGURE 12 Predicted ice volume fraction distribution from center to surface. (a): condition A1 (constant at −21°C). (b) Condition A3 (fluctuating from −21°C to −17°C). (c) Condition A2 (fluctuating from −21°C to −13°C)
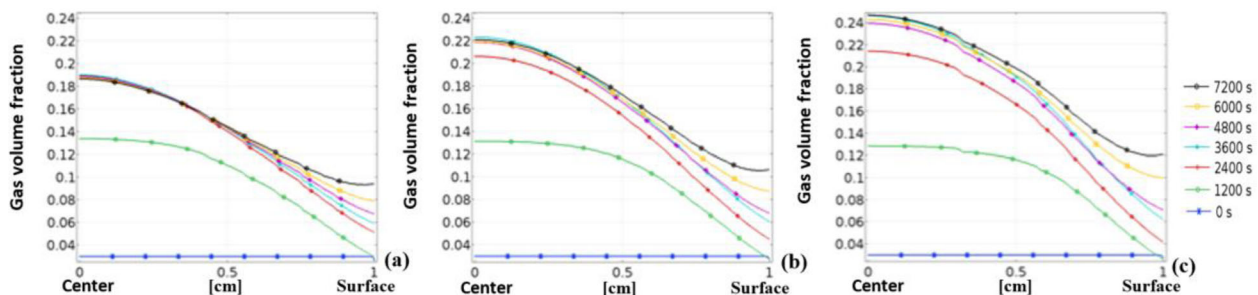

FIGURE 13 Gas volume fraction distribution from center to surface. (a) Condition A1 (constant at −21°C). (b) Condition A3 (fluctuating from −21°C to −17°C). (c) Condition A2 (fluctuating from −21°C to −13°C)
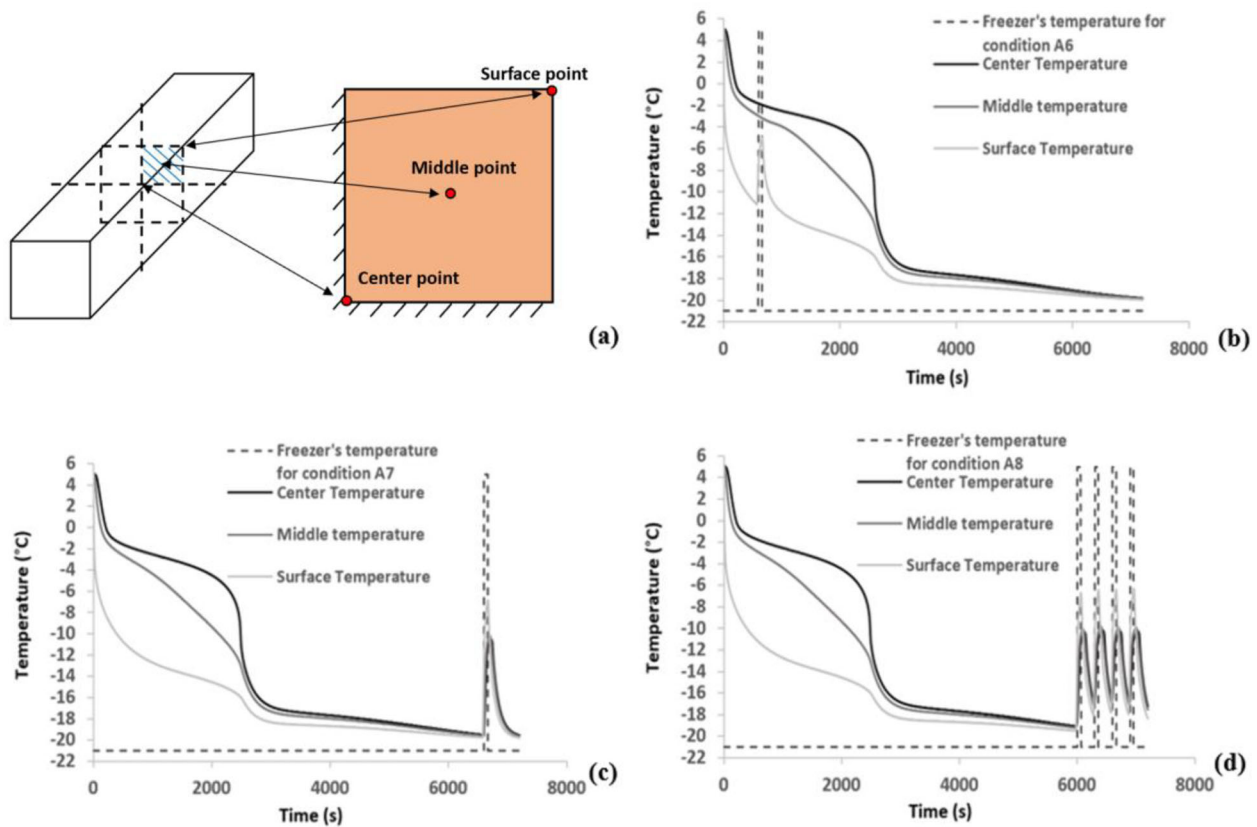
FIGURE 14   Calculated results for center, middle, and surface temperature profiles for different open-close conditions. (b) Condition A6, (c) condition A7, (d) condition A8

industry should avoid frequent changes in freezing temperature. Data for conditions A4 and A5 showed similar trends and is presented in Zhao (2019).

7.4.5 | Opening and closing freezer's door application

In day-to-day life, temperature fluctuations would occur due to consumers' opening and closing freezer doors. The fluctuation in temperature caused by opening and closing of doors is expected to defrost the ice on the surface and damage the quality of the frozen products. We used our model to simulate three opening and closing conditions by changing the ambient air temperature outside a frozen potato in the solution scheme to investigate their effect on fluid transport and ice formation. The condition A6 represented the freezer temperature changing to $5°C$ between 600 s and 660 s and approaching $-21°C$ for the remaining simulation time following the profile shown in Figure 14b. Condition A7 shows a sudden temperature increase to $5°C$ between 6600 s and 6660 s (Figure 14c). Condition A8 shows the freezer subjected to multiple open-close situations with temperature rising to $5°C$ from 6000 s to 6060

s, 6300 s to 6360 s, 6600 s to 6660 s, and 6900 s to 6960 s, and was $-21°C$ for the remaining time (Figure 14d). The variation in heat transfer coefficient due to change in air flow patterns due to opening and closing of doors was not included. Door opening and closing was included simply by changing temperature in air around the samples. The surface temperatures for conditions A6, A7, and A8 showed the expected increase in response to the sudden rise in ambient temperature (Figure 15). The center temperature for condition A6 was not disturbed by the sudden blip of temperature occurring on the surface. The plot for temperature distribution from center to surface would be a better illustration to see how the blip in ambient temperature would affect the temperature inside the material.

Figure 15a shows that the temporary temperature rises near the surface only spread about 0.2 cm (0.8 to 1 cm) inside the sample between 600 s and 660 s. The inner part (0 to 0.5 cm) was still experiencing freeze plateau and its temperature stayed around the freezing point. Since phase change requires a large amount of latent heat, the center was shielded from the sudden temperature rise occurring near the surface. Therefore, the center for condition A6 does not manifest a temperature rise. For conditions A7 and A8, the intermittent temperature rise occurred
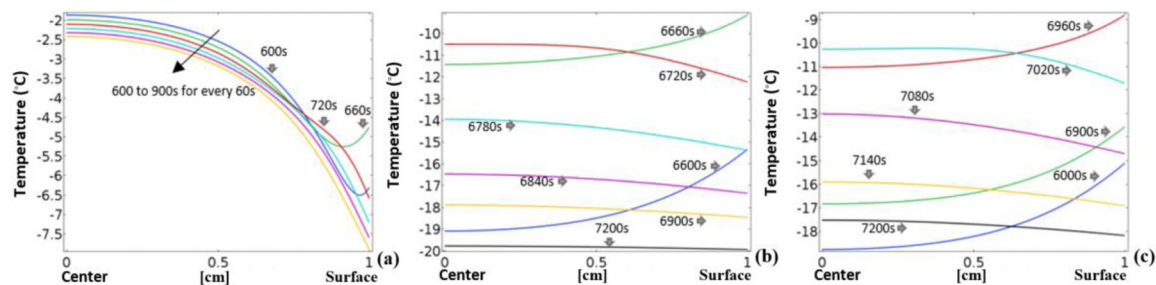
FIGURE 15 Temperature distribution from center to surface at different time. (a) Condition A6, (b) condition A7, (c) condition A8
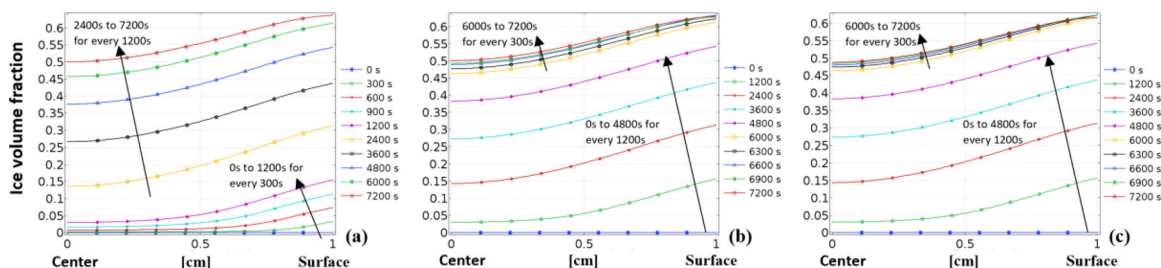

FIGURE 16 Ice volume fraction distribution from center to surface at different times. (a) Condition A6, (b) condition A7, (c) condition A8

when the whole material had reached the set freezing temperature around $-21°$C.

The average volume fraction of ice rose above 0.56 after 6000 s (average ε^i was only 0.05 at 600 s). When the phase change had almost finished and no more latent heat was being discharged, heat was easier to transfer inside the material and produced the material's temperature increase. As a result, the center temperature in the sample was affected and increased from $-19°$C to $-11.5°$C, as the ambient temperature rose between 6600 s and 6660 s (Figure 16b). The simulation results indicated that the sudden temperature fluctuation had a more critical effect after the frozen foods passed through the phase change period and large amounts of ice had formed inside.

Figure 16 exhibits the ice distribution plots from center to surface in the geometry for these conditions. For condition A6 (Figure 16a), the ice formation was not affected by the sudden temperature rise between 600 s and 660 s, and the ice distribution profile was almost the same as the plot for condition A1 (Figure 12). For condition A7, the ice content stopped increasing after 6600 s. The curve at 6900 s overlapped with that of 6600 s, and the final content at 7200 s was only slightly higher than for the previous time points (Figure 16b). For condition A8, the results of ice volume fraction distribution from center to surface were hardly distinguishable from each other after 6000 s. The average of ε^i at 7200 was less than the amount at 6000

s (Figure 16c). This is expected to have been caused by the rise and fall of the ambient temperature, which caused lowering of ice content near the surface.

This phenomenon can also be explained from the perspective of the ice formation rate (Figure 17). The water and ice mass exchange rate $^w\hat{e}^i$ was controlled by the difference of partial pressures between the water and in the vicinity of ice phases. The vapor pressure in the vicinity of ice decreased when the temperature became lower (Chen, 1987; Fennema, 1996). The vapor pressure of water was related to the product of water activity and equilibrium saturated pressure at a specific temperature (Takhar, 2014). When most of the water had been transferred to ice, the water activity was reduced, and saturated pressure was also smaller. The ice formation rate became negative, which prompted the ice to melt, which may deteriorate the frozen foods' quality.

The results discussed above indicate that the frozen shipping systems need to operate such that the whole food is allowed to be frozen before it is shipped and dispersed. Once the whole food is frozen, the sudden temperature fluctuation can still affect the inner temperature of a frozen material. Multiple opening–closing situations would result in more damage to the frozen foods' quality compared to the one with fewer fluctuations. To reduce melting of surface layers, the amplitude and frequency of freeze–thaw cycles need to be reduced.
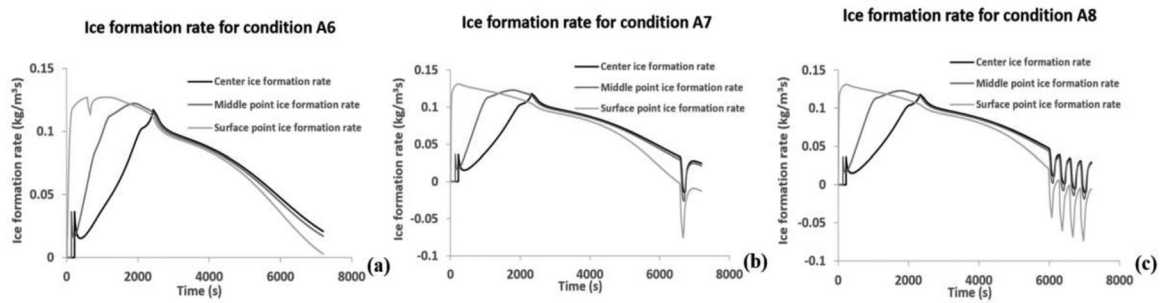
FIGURE 17 Ice formation rate at center, middle and surface point. (a) Condition A6. (b): condition A7, (c) condition A8

8 | CONCLUSIONS

The freezing of biopolymers was modeled by solving the HMT-based two-scale equations of fluid, species, and heat transport coupled with a physical chemistry-based relation. The volume change during freezing was included using the stresses generated from pore pressure and thermal strain due to fluid migration and phase change. The model was applied to investigate the freezing process in a French fry-shaped potato. A good agreement with experimental results was achieved for both constant and fluctuating freezing conditions (RMSE are 2.86°C and 2.23°C, respectively). The numerical results of the freezing process revealed that the freezing point depression is characterized by the species transport in the unfrozen fluid. Lower freezing rate and higher mass loss were observed for the air blast freezer compared to the liquid ethylene glycol freezing medium. Different fluctuating cycles strongly influenced the ice formation and gas distribution during freezing. The simulation results revealed that larger magnitudes of temperature fluctuations cause more gas content at the center than that of the constant freezing condition after 2 h of freezing, which can contribute to larger pores. The model was also effectively employed to simulate the opening and closing of freezer doors. The multiple opening–closing of freezer door occurring after the material went through phase change were observed to produce ice melting and matrix geometry instability, which can make the food prone to undesirable quality changes. Overall, the HMT-based model of mass, species, and heat transfer provided a viable approach and physical insights for the problems involving multi-constituent, diverse geometries, and complex boundary conditions during freezing for both scientific and practical significance.

Nomenclature

a_w	water activity (dimensionless)
C_p^α	heat capacity of phase α (J/[kg·K])
C_{pLH}	heat capacity of latent heat (J/[kg·K])
D_{ia}	Dimension of the material (m)
D^α	diffusivity of fluid phase in the biopolymeric matrix ([m²/s])
D^{w_j}	diffusivity of solute j in the fluid phase (m²/s)
E	Young's modulus or coefficient of elasticity (Pa)
$^\beta \hat{e}^\alpha$	net rate of mass transferred from the β-phase to α-phase (kg/[m³·s])
F_b	body force (N/m³)
h_c	heat transfer coefficient (W/[m²·K])
h_m	mass transfer coefficient (m/s)
$\boldsymbol{I}$	identity matrix
j	jth species
j^s	Jacobian matrix (dimensionless)
k^α	thermal conductivity of the α-phase (W/[m·K])
K^g	permeability of the gas phase (m²)
K^w	permeability of the water phase (m²)
L_f	latent heat of freezing (J/kg)
L_v	latent heat of vaporization (J/kg)
M^α	molecular weight of the α-phase (kg/mol)
m^α	mass weight of the α-phase (kg/mol)
m^j	mass weight of the solute j (kg/mol)
Nu	Nusselt number (dimensionless)
p_{atm}	atmospheric pressure (Pa)
p^{cw}	capillary pressure of water in pore (Pa)
p_{pore}	pore pressure (Pa)
Pr	Prandtl number (dimensionless)
p_{sat}	saturated vapor pressure (Pa)
p_{eq}^v	pressure of vapor phase at equilibrium (Pa)
P^α	partial pressure of the α-phase (Pa)
Q_w	Mass flux for the boundary condition of water phase equation (kg/(m²·s)]
Q_T	Heat flux for the boundary condition of energy balance (W/m²)
Q_v	Mass flux for the boundary condition of vapor phase equation (kg/[m²·s])
REV	representative elementary volume (m³)
R^v	universal gas constant (J/[K·mol])
Re	Reynolds number (dimensionless)
R_H	relative humidity (fraction)
s^α	degree of the saturation by the α-phase (dimensionless)
t	time (s)

T	temperature (K or °C)
T_f	freezing point (K or °C)
T_{amb}	freezer temperature (K or °C)
u	displacement field (m)
u_f	velocity of fluid diffusion (m/s)
v^s	velocity of solid phase for matrix changing (m/s)
$v^{\alpha,s}$	velocity of the α-phase with respect to solid phase (m/s)
$v^{w_j,s}$	velocity of the solute j in the fluid phase to solid phase (m/s)
V^α	volume occupied by the α-phase (m³)
X_w	mass fraction of water in dry basis (kg water/kg solid)
α_m	mass fraction factor for phase change (dimensionless)
$\alpha(T)$	thermal expansion coefficient (1/K)
δ_{ij}	Kronecker delta (dimensionless)
ξ	evaporation rate constant (1/s)
ζ	displacement coefficient (dimensionless)
ε^α	volume fraction of the α-phase (dimensionless)
μ^α	viscosity of the α-phase (Pa/s)
ρ^α	density of the α-phase (kg/m³)
ρ^{w_j}	density of the solute j in the fluid phase (kg/ m³)
σ	stress tensor (Pa)
ϕ	porosity of the material (dimensionless)
ω^v	mass fraction of water vapors (dimensionless)
E_{KK}	normal components of Lagrangian strain tensor, K=X, Y,Z (dimensionless)
α	general representation of a phase
β	general representation of a phase other than α
a	air
i	ice phase
g	gas phase
s	solid phase
v	water vapors
w	water phase
o	initial
atm	atmosphere
avg	average
E	Eulerian coordinate
exp	experimental
eq	equilibrium
L	Lagrangian coordinate
$phch$	phase change
sat	saturated
dv	Eulerian volume of the material (m³)
dV	Lagrangian volume of the material (m³)
∇_E	spatial gradient in Eulerian coordinate (1/m)
∇_L	spatial gradient in Lagrangian coordinate (1/m)
ΔT_f	freezing point depression (K)
Dot	$(\cdot)$ material time derivative following the solid phase motion D^s/Dt (1/s)

AUTHOR CONTRIBUTIONS

Ying Zhao: formal analysis; investigation; methodology; validation; visualization; writing – original draft. **Pavitra Krishna Kumar**: data curation; formal analysis; investigation; methodology; writing – original draft. **Shyam S. Sablani**: funding acquisition; investigation; methodology; project administration; supervision; writing – review & editing. **Pawan S. Takhar**: conceptualization; formal analysis; funding acquisition; investigation; project administration; supervision; validation; writing – review & editing.

CONFLICT OF INTEREST

The authors declare no conflict of interest.

ORCID

Shyam S. Sablani https://orcid.org/0000-0001-5602-3832

Pawan S. Takhar https://orcid.org/0000-0002-2617-0767

REFERENCES

Achanta, S., Cushman, J. H., & Okos, M. R. (1994). On multicomponent, multiphase thermomechanics with interfaces. *International Journal of Engineering Science*, *32*(11), 1717–1738.

Acheson, D. J. (1991). *Elementary fluid dynamics* (pp. 205). Acoustical Society of America.

Adapa, S., Schmidt, K., Jeon, I., Herald, T., & Flores, R. (2000). Mechanisms of ice crystallization and recrystallization in ice cream: A review. *Food Reviews International*, *16*(3), 259–271.

Andreas, E. L. (2005). *Handbook of physical constants and functions for use in atmospheric boundary layer studies.* Cold Engineering Research and Engineering Laboratory, U.S. Army Engineer Research and Development Center.

Atkins, P., & De Paula, J. (1998). *Physical chemistry* (Vol. 4). Oxford University Press.

Bansal, H. S., Takhar, P. S., Alvarado, C. Z., & Thompson, L. D. (2015). Transport mechanisms and quality changes during frying of chicken nuggets—Hybrid mixture theory based modeling and experimental verification. *Journal of food science*, *80*(12), E2759–E2773.

Bansal, H. S., Takhar, P. S., & Maneerote, J. (2014). Modeling multiscale transport mechanisms, phase changes and thermomechanics during frying. *Food Research International*, *62*, 709–717.

Bartolome, L. G., & Hoff, J. E. (1972). Firming of potatoes. Biochemical effects of preheating. *Journal of Agricultural and Food Chemistry*, *20*(2), 266–270.

Battiato, I., Ferrero, P. T., O'Malley, D., Miller, C. T., Takhar, P. S., Valdes-Parada, F. J., & Wood, B. D. (2019). Theory and applications of macroscale models in porous media. *Transport in Porous Media*, *130*(1), 5–76. https://doi.org/10.1007/s11242-019-01282-2

Baxter, P., & West, D. (1977). The flow of water into fruit trees. I. Resistances to water flow through roots and stems. *Annals of Applied Biology*, *87*(1), 95–101.

Bear, J., & Bachmat, Y. (2012). *Introduction to modeling of transport phenomena in porous media* (Vol. 4). Springer Science & Business Media.

Bennethum, L. S., & Cushman, J. H. (1996). Multiscale, hybrid mixture theory for swelling systems—I: Balance laws. *International Journal of Engineering Science*, *34*(2), 125–145.

Bird, R. B., Stewart, W. E., & Lightfoot, E. N. (2002). *Transport phenomena*. Wiley.

Bird, R. B., Stewart, W. E., & Lightfoot, E. N. (2007). *Transport phenomena* (Revised 2nd ed.). John Wiley & Sons.

Bonacina, C., Comini, G., Fasano, A., & Primicerio, M. (1973). Numerical solution of phase-change problems. *International Journal of Heat and Mass Transfer*, *16*(10), 1825–1832.

Bradshaw, J. E., & Bonierbale, M. (2010). Potatoes. In *Root and tuber crops* (pp. 1–52): Springer.

Cengel, Y. A., Klein, S., & Beckman, W. (1998). *Heat transfer: A practical approach* (Vol. 141). WBC McGraw-Hill Boston.

Chiam, H., Azmi, W., Usri, N., Mamat, R., & Adam, N. (2017). Thermal conductivity and viscosity of Al2O3 nanofluids for different based ratio of water and ethylene glycol mixture. *Experimental Thermal and Fluid Science*, *81*, 420–429.

Chen, C. (1986). Effective molecular weight of aqueous solutions and liquid foods calculated from the freezing point depression. *Journal of Food Science*, *51*(6), 1537–1539.

Chen, C. (1987). Relationship between water activity and freezing point depression of food systems. *Journal of Food Science*, *52*(2), 433–435.

Chen, P., Chen, X. D., & Free, K. W. (1996). Measurement and data interpretation of the freezing point depression of milks. *Journal of Food Engineering*, *30*(1–2), 239–253.

Chen, X. D., & Chen, P. (1996). Freezing of aqueous solution in a simple apparatus designed for measuring freezing point. *Food Research International*, *29*(8), 723–729.

Conrad, F. H., Hill, E., & Ballman, E. (1940). Freezing points of the system ethylene glycol–methanol–water. *Industrial & Engineering Chemistry*, *32*(4), 542–543.

Delgado, A., & Sun, D.-W. (2001). Heat and mass transfer models for predicting freezing processes—A review. *Journal of Food Engineering*, *47*(3), 157–174.

Dempsey, P., & Bansal, P. (2012). The art of air blast freezing: Design and efficiency considerations. *Applied Thermal Engineering*, *41*, 71–83.

Ditudompo, S., & Takhar, P. S. (2015). Hybrid mixture theory based modeling of transport mechanisms and expansion-thermomechanics of starch during extrusion. *AIChE Journal*, *61*(12), 4517–4532.

Ehlers, W. (2002). *Porous media: Theory, experiments and numerical applications*. Springer Science & Business Media.

Fang, G., & Ward, C. (1999). Temperature measured close to the interface of an evaporating liquid. *Physical Review E*, *59*(1), 417.

Farid, M. (2002). The moving boundary problems from melting and freezing to drying and frying of food. *Chemical Engineering and Processing: Process Intensification*, *41*(1), 1–10.

Feng, H., Tang, J., Plumb, O., & Cavalieri, R. (2004). Intrinsic and relative permeability for flow of humid air in unsaturated apple tissues. *Journal of Food Engineering*, *62*(2), 185–192.

Fennema, O. R. (1996). Water and ice. In *Food science and technology* (pp. 17–94). Marcel Dekker.

Finney, E., & Hall, C. (1967). Elastic properties of potatoes. *Transactions of the ASAE*, *10*(1), 4–8.

Fukusako, S. (1990). Thermophysical properties of ice, snow, and sea ice. *International Journal of Thermophysics*, *11*(2), 353–372.

Gabas, A., Telis-Romero, J., & Telis, V. (2003). Influence of fluid concentration on freezing point depression and thermal conductivity of frozen orange juice. *International Journal of Food Properties*, *6*(3), 543–556.

Grant, S. A., & Sletten, R. S. (2002). Calculating capillary pressures in frozen and ice-free soils below the melting temperature. *Environmental Geology*, *42*(2–3), 130–136.

Halder, A., Dhall, A., & Datta, A. (2007). An improved, easily implementable, porous media based model for deep-fat frying: Part I: Model development and input parameters. *Food and Bioproducts Processing*, *85*(3), 209–219.

Hassanizadeh, S. M., & Gray, W. G. (1979). General conservation equations for multiphase systems: 1. Averaging procedure. *Advances in Water Resources*, *2*, 131–144.

Heldman, D. R. (1982). Food properties during freezing. 92–96.

Heldman, D., & Taylor, T. (1997). Modeling of food freezing. In *Quality in frozen food* (pp. 51–64). Springer.

Heldman, D. R., Lund, D. B., & Sabliov, C. (2018). *Handbook of food engineering*. CRC Press.

Iyahraja, S., & Rajadurai, J. S. (2015). Study of thermal conductivity enhancement of aqueous suspensions containing silver nanoparticles. *AIP Advances*, *5*(5), 057103.

Kumar, P. K., Bhunia, K., Tang, J., Rasco, B. A., Takhar, P. S., & Sablani, S. S. (2018). Thermal transition and thermo-physical properties of potato (*Solanum tuberosum* L.) var. Russet brown. *Journal of Food Measurement and Characterization*, *12*(3), 1572–1580.

Kumar, P. K., Bhunia, K., Tang, J., Rasco, B. A., Takhar, P. S., & Sablani, S. S. (2019). State/phase transitions induced by ice recrystallization and its influence on the mechanical properties of potatoes (*Solanum tuberosum* L.) var. Russet Brown. *Journal of Food Engineering*, *251*, 45–56.

La Placa, S., & Post, B. (1960). Thermal expansion of ice. *Acta Crystallographica*, *13*(6), 503–505.

Le-Bail, A., Chapleau, N., Anton-De Lamballerie, M., & Vignolle, M. (2008). Evaluation of the mean ice ratio as a function of temperature in a heterogeneous food: Application to the determination of the target temperature at the end of freezing. *International Journal of Refrigeration*, *31*(5), 816–821.

Manga, M., & Wang, C. Y. (2007). Pressurized oceans and the eruption of liquid water on Europa and Enceladus. *Geophysical Research Letters*, *34*(7), 1–5.

McKellar, A., Paterson, J., & Pham, Q. T. (2009). A comparison of two models for stresses and strains during freezing. *Journal of Food Engineering*, *95*, 142–150.

Möller, D. (2014). *Chemistry of the climate system*. Walter de Gruyter GmbH & Co KG.

Netti, P., Travascio, F., & Jain, R. (2003). Coupled macromolecular transport and gel mechanics: Poroviscoelastic approach. *AIChE Journal*, *49*(6), 1580–1596.

Newman, G. P., & Wilson, G. W. (1997). Heat and mass transfer in unsaturated soils during freezing. *Canadian Geotechnical Journal*, *34*(1), 63–70.

Perry, R. H., & Green, D. W. (1997). *Perry's chemical engineers' handbook* (7th ed.). McGraw Hill.

Peyghambarzadeh, S., Hashemabadi, S., Hoseini, S., & Jamnani, M. S. (2011). Experimental study of heat transfer enhancement using water/ethylene glycol based nanofluids as a new coolant for car radiators. *International Communications in Heat and Mass Transfer*, *38*(9), 1283–1290.

Pham, Q. T. (1986). Simplified equation for predicting the freezing time of foodstuffs. *International Journal of Food Science & Technology*, *21*(2), 209–219.

Pham, Q. T. (2006). Modelling heat and mass transfer in frozen foods: A review. *International Journal of Refrigeration*, *29*(6), 876–888.

Pham, Q. T. (2008). Advances in food freezing/thawing/freeze concentration modelling and techniques. *Japan Journal of Food Engineering*, *9*(1), 21–32.

Pham, Q. T. (2016). Freezing Theory. In Caballero, B., Finglas, P. M., & Toldrá, F. (Eds.), *Encyclopedia of food and health* (pp. 110–118). Academic Press.

Poling, B. E., Prausnitz, J. M., & O'connell, J. P. (2001). *The properties of gases and liquids*. McGraw-Hill.

Poon, G. G., & Peters, B. (2013). A stochastic model for nucleation in the boundary layer during solvent freeze-concentration. *Crystal Growth & Design*, *13*(11), 4642–4647.

Reeb, J. E., Milota, M. R., & Association, W. D. K. (1999). Moisture content by the oven-dry method for industrial testing. *In 50th Western Dry Kiln Association Meeting*, *5*, 66–74.

Rouaud, O., & Pham, Q. (2012). Heat and mass transfer modelling during freezing of foodstuffs. In *The proceedings of the COMSOL conference*, Milan, Italy.

Saravacos, G. (1967). Effect of the drying method on the water sorption of dehydrated apple and potato. *Journal of Food Science*, *32*(1), 81–84.

Saravacos, G., & Stinchfield, R. (1965). Effect of temperature and pressure on the sorption of water vapor by freeze-dried food materials. *Journal of Food Science*, *30*(5), 779–786.

Selvam, C., Lal, D. M., & Harish, S. (2017). Thermal conductivity and specific heat capacity of water–ethylene glycol mixture-based nanofluids with graphene nanoplatelets. *Journal of Thermal Analysis and Calorimetry*, *129*(2), 947–955.

Sharma, A. (2014). Global frozen food market trends and forecasts to 2020. https://www.linkedin.com/pulse/20141118100129-214337948-global-frozen-food-market-trends-and-forecasts-to-2020/

Singh, P. P., Cushman, J. H., & Maier, D. E. (2003a). Multiscale fluid transport theory for swelling biopolymers. *Chemical Engineering Science*, *58*(11), 2409–2419.

Singh, P. P., Cushman, J. H., & Maier, D. E. (2003b). Three scale thermomechanical theory for swelling biopolymeric systems. *Chemical Engineering Science*, *58*(17), 4017–4035.

Spolek, G., & Plumb, O. (1981). Capillary pressure in softwoods. *Wood Science and Technology*, *15*(3), 189–199.

Sun, D.-W. (2016). *Handbook of frozen food processing and packaging*. CRC Press.

Stanish, M., Schajer, G., & Kayihan, F. (1986). A mathematical model of drying for hygroscopic porous media. *AIChE Journal*, *32*(8), 1301–1311.

Szymońska, J., & Wodnicka, K. (2005). Effect of multiple freezing and thawing on the surface and functional properties of granular potato starch. *Food Hydrocolloids*, *19*(4), 753–760.

Takhar, P. S. (2014). Unsaturated fluid transport in swelling poroviscoelastic biopolymers. *Chemical Engineering Science*, *109*, 98–110.

Usri, N., Azmi, W., Mamat, R., Hamid, K. A., & Najafi, G. (2015). Thermal conductivity enhancement of Al_2O_3 nanofluid in ethylene glycol and water mixture. *Energy Procedia*, *79*, (Supplement C), 397–402.

Vafai, K., & Tien, H. (1989). A numerical investigation of phase change effects in porous materials. *International Journal of Heat and Mass Transfer*, *32*(7), 1261–1277.

Vargaftik, N. B. (1975). Tables on the thermophysical properties of liquids and gases. *Hemisphere Corp*, (pp. 99). Washington, DC, United States.

Voller, V. R., & Prakash, C. (1987). A fixed grid numerical modelling methodology for convection-diffusion mushy region phase-change problems. *International Journal of Heat and Mass Transfer*, 30(8), 1709–1719.

Voller, V. R., Swaminathan, C., & Thomas, B. G. (1990). Fixed grid techniques for phase change problems: A review. *International Journal for Numerical Methods in Engineering*, *30*(4), 875–898.

Wollhöver, K., Körber, C., Scheiwe, M., & Hartmann, U. (1985). Unidirectional freezing of binary aqueous solutions: An analysis of transient diffusion of heat and mass. *International Journal of Heat and Mass Transfer*, *28*(4), 761–769.

Zábranský, M., Růžička Jr, V., & Domalski, E. S. (2001). Heat capacity of liquids: Critical review and recommended values. Supplement I. *Journal of Physical and Chemical Reference Data*, *30*(5), 1199–1689.

Zhao, Y. (2019). *Multiscale modeling of transport mechanisms and quality changes in frozen foods during freeze-thaw cycles* (Ph.D. Thesis). Agricultural & Biological Engr, University of Illinois at Urbana-Champaign.

Zhao, Y., & Takhar, P. S. (2017a). Freezing of foods: Mathematical and experimental aspects. *Food Engineering Reviews*, *9*(1), 1–12.

Zhao, Y., & Takhar, P. S. (2017b). Micro X-ray computed tomography and image analysis of frozen potatoes subjected to freeze-thaw cycles. *LWT – Food Science and Technology*, *79*, 278–286.

Zogzas, N., Maroulis, Z., & Marinos-Kouris, D. (1996). Moisture diffusivity data compilation in foodstuffs. *Drying Technology*, *14*(10), 2225–2253.

Zorrilla, S. E., & Rubiolo, A. C. (2005). Mathematical modeling for immersion chilling and freezing of foods: Part II: Model solution. *Journal of Food Engineering*, *66*(3), 339–351.